 doi:10.20944/preprints202103.0720.v1

Review

Microneedle arrays for sampling and sensing dermal interstitial fluid

Navid Kashaninejad[1,*], Ahmed Munaz[1#], Hajar Moghadas[2#], Sharda Yadav[1#], Muhammad Umer[1#] and Nam-Trung Nguyen [1,*]

[1] Queensland Micro- and Nanotechnology Centre, Nathan Campus, Griffith University, 170 Kessels Road, Brisbane QLD 4111, Australia. munaz.ahmed@griffith.edu.au (A.M.); s.yadav@griffith.edu.au (S. Y.); m.umer@griffith.edu.au (M.U.)

[2] Department of mechanical engineering, Gas and Petroleum Faculty, Yasouj University, 75918-74831, Iran. h.moghadas@yu.ac.ir (H.M.)

* Correspondence: n.kashaninejad@griffith.edu.au; Tel.: +61 7373 55391. nam-trung.nguyen@griffith.edu.au; Tel.: +61 7373 53921.

\# These authors contributed equally to this work

Abstract: Dermal interstitial fluid (ISF) is a novel source of biomarkers that can be considered as an alternative to blood sampling for disease diagnosis and treatment. Nevertheless, *in vivo* extraction and analysis of ISF are challenging. On the other hand, microneedle (MN) technology can address most of the challenges associated with dermal ISF extraction and is well-suited for long-term, continuous ISF monitoring as well as *in situ* detection. In this review, we first briefly summarise the different dermal ISF collection methods and compare them with MN methods. Next, we elaborate on the design considerations and biocompatibility of MNs. Subsequently, the fabrication technologies of various MNs used for dermal ISF extraction, including solid MNs, hollow MNs, porous MNs and hydrogel MNs, are thoroughly explained. In addition, different sensing mechanisms of ISF detection will be discussed in detail. Subsequently, we identify the challenges and propose the possible solutions associated with ISF extraction. A detailed investigation is provided for the transport and sampling mechanism of ISF *in vivo*. Also, the current *in vitro* skin model integrated with the MN arrays will be discussed. Finally, future directions to develop a point-of-care (POC) device to sample ISF are proposed.

Keywords: microneedle; microneedle array, interstitial fluid; bio sensing, wearable system; ISF sampling

1. Introduction

Interstitial fluid (ISF) is a novel source of biomarkers. The ISF flow through the extracellular matrix of tissue between the blood and lymphatic vessels [1]. Almost 60-70% of the body fluid content is constituted by the ISF [2]. ISF transports the necessary protein through the interstitium and contributes to microcirculation around the cell matrix. The fluid provides a suitable mechanical environment and physiological activities for the interstitial cells [3]. ISF delivers nutrients and transfers external stimuli to the cells in the region. The ISF also works as a carrier to remove waste products [4].

ISF can be a great alternative to blood due to the presence of small molecules such as glucose, lactate, cortisol, and urea [5]. Observing the molecular concentration in ISF and its flow pattern can provide important information about specific diseases. For instance, the changes in fluid pressure and volume in the ISF can be an indication of kidney diseases. ISF pressure is negative in healthy controls (-0.9 mm Hg) compared to an elevated pressure of almost 4.6 mm Hg for chronic kidney disease [6]. Besides, insulin deficiency is observed in diabetic patients resulting in a higher or lower glucose level (normal range 80-120 mg/dL) in blood and ISF [7]. The consequences could be severe as the glucose

 doi:10.20944/preprints202103.0720.v1

intake by the tissue drastically reduces. This is due to the decreased working function of insulin in the body.

Furthermore, the progression of cancer increases the intratumoral pressure that changes the surrounding microenvironments [8,9]. Such an issue affects the drainage of ISF through the lymphatic vasculature downstream, resulting in an increased level of flow from the bulk tumour to the healthy stroma. ISF flow increases noticeably in the presence of breast carcinoma, metastatic melanoma, head and neck carcinoma tumours [10,11]. As the tumour grows and metastasises to the surrounding environment, they acquire more nutrient supply through blood vessel networks [12]. In addition, an increased amount of ISF from the tumour also contributes to the leakage of blood vessels, abnormalities in the lymph-vessel, and contraction in the interstitial space from the stromal fibroblasts [13]. A certain drop in ISF flow could be an indication of abnormalities in the patient's body. For instance, burn injuries or inflammations in the patients could drastically reduce the pattern of ISF flow.

Therefore, observing, sampling, and extracting the ISF will be very beneficial for non-invasive monitoring of patients' health. Detecting the reliable concentration of specific biomarkers from the ISF-based point-of-care (POC) unit will make the clinical assays extremely easy and affordable for drug quantification. The long-term and continuous monitoring required with chronic kidney disease and diabetes will be easy to control without causing any patients' discomfort [14].

Because the skin is the most accessible organ in the human body, sampling dermal ISF is the most practical way for biosensing applications. Conventionally, dermal ISF is collected using suction blister, iontophoresis, sonophoresis and microdialysis. These techniques are relatively invasive, time-consuming, and require expert skills to be performed; otherwise, they may lead to permanent skin damage.

Alternatively, microfluidic technology can address the limitations associated with conventional ISF sampling techniques. Microfluidics is an emerging science and technology that can offer significant improvements over various fields, including surface science [15], nanotechnology for disease diagnosis [16], mixing [17] and separation [18,19], mechanobiology [20], cancer research [21,22], cell culture [23,24], single-cell analysis [25], drug delivery at cellular [26] and tissue levels [27], electrochemical biosensing [28], and POC sensing [29]. Furthermore, the emerging field of micro elastofluidics can provide microfluidic solutions for flexible, conformal system attached to the skin [26]. In the context of dermal ISF collection and sensing, microfluidics can be used in three different formats: (i) Passive microneedles (MNs) for merely collecting the dermal ISF painlessly; (ii) Active MNs integrated with sensor to both collect dermal ISF and actively sense the target analyte of interest *in situ*; (iii) More realistic *in vitro* model of the skin for ISF flow. The first application is in line with the advances in drug delivery and vaccine administration. The second application, i.e., using MNs for both ISF collection and sensing, has been mainly investigated for continuous glucose monitoring as a part of wearable POC devices for diabetes. Nevertheless, the third application has received less attention among the scientific community and will be highlighted in this review paper.

In 1998, the first use of MNs, with a length of 150 μm, for transdermal drug delivery was reported [30]. Since then, MNs have extensively been used for vaccine and drug delivery as a part of lab-on-a-chip devices at the organ level [31]. Recently, the applications of MNs for sampling ISF and measuring the unique biomarkers for disease diagnosis, prognosis and treatment monitoring have attracted a great deal of attention [32]. Most importantly, the surface of the MNs can act as a biosensor when functionalised with bio-recognition elements such as peptides, antibodies, and antigens to directly interact with the target of interest in the ISF. This can be considered as a paradigm shift for POC and *in situ* disease detection and longitudinal monitoring [33]. Accordingly, a new research field, called "lab under the skin" has been coined that mainly refers to the applications of wearables, MN-based transdermal sensors [34].

While MNs can potentially be used to detect and monitor various biotargets such as urea, lactate, amino acids, alcohol and therapeutic agents, they have been extensively used

Preprints (www.preprints.org) | NOT PEER-REVIEWED | Posted: 30 March 2021 doi:10.20944/preprints202103.0720.v1

for glucose monitoring [35]. The applications of electrochemical MNs for the detection of most of these biotargets have recently been reviewed [36]. Moreover, the advantages and challenges of using electrochemical MNs for *in vivo* ISF extraction have been thoroughly discussed elsewhere [37]. Nevertheless, there is still a lack of a comprehensive review paper that systematically investigates the design consideration, fabrication, and sensing applications of MNs for ISF extraction and monitoring.

Herein, we discuss the challenges and possible solutions currently associated with the extraction of ISF. A detailed investigation is addressed for the transport and sampling mechanism of the ISF *in vivo*. The current *in vitro* skin model integrated with the MN array is discussed. Finally, future direction to develop a POC device to sample ISF is proposed.

2. Sampling methods for ISF collection

ISF is an attractive source of unique biomarkers due to the absence of clotting factors. The fluid contains biochemical information such as the number of electrolytes, proteins, peptides, and metal ions. It is necessary to understand the transport mechanism of ISF in the human body. The transport of fluid and solute molecule in tissue was first explained by Starling's hypothesis [38]. The hypothesis suggests that the fluid is filtered through the arterial end of a vessel and reabsorbed at the venous end. ISF is an incompressible Newtonian fluid. The viscosities changes with pressure, temperature, and incorporation of external chemical species.

The interstitial fluid flow can be modelled by defining the interstitial cells called mast cells. The mast cells are an immune cell mostly found in connective tissues [39]. The mast cells have a thin boundary layer on the cell surface, named the Brinkman boundary layer. The space between the interstitium consists of collagen fibrils which are porous media. The stimulated mast cells release chemical mediators from their cellular granules into the extracellular matrix. This causes a series of biological responses [1]. The flow of the ISF can be defined by the Brinkman and Continuity equations as [40]:

$$\nabla p = \mu \Delta \vec{v} - \frac{\mu}{k_p} \vec{u}, \tag{1}$$

$$\nabla . \vec{v} = \vec{0}, \tag{2}$$

Here ∇ is the gradient operator, Δ is the Laplacian operator, $\vec{v}$ is the velocity vector, p is the pressure in the interstitium, μ is the viscosity of the ISF, and k_p is the Darcy permeability of the collagen fibrin matrix. Samant *et al.* demonstrated that the extraction of ISF dramatically depends on the transport mechanism [41]. According to their findings, the pressure-gradient between the skin layer can collect a significant amount of ISF within a short time compared to the osmosis, capillary action, and diffusion technique. The pressure gradient can be generated by introducing higher molecular weight osmolyte with low diffusivity in the surrounding ISF. Besides, pulsating vacuum pressure with an appropriate MNs array can provide long term steady pressure gradient. Thus, ample ISF can be extracted for long hours for continuous investigations. However, skin tolerance to pressure needs to be optimised. Gradual ramping of the pressure can reduce skin damage by many folds.

ISF can be collected and analysed in three possible routes. Figure 1 shows the schematic of the possible three routes in a skin model. Transcellular routes extract or analyse the ISF directly through the cells [42]. Injecting needles is one of the ways in this approach. The needle penetrates through the alternative lipophilic and hydrophilic layers and reaches into the dermal region. The intercellular route utilises the intercellular space between the cells. The intercellular space consists of cholesterol, ceramides, and free fatty acids. Suction blister and iontophoresis are examples of this approach. The last method is to utilise the appendageal route of the skin, such as the hair follicles and glands. However, this route is neglected for ISF collection since hair follicles and glands are small and are present in limited parts of the human skin.

Preprints (www.preprints.org) | NOT PEER-REVIEWED | Posted: 30 March 2021 doi:10.20944/preprints202103.0720.v1

Research has shown that permeation and extraction through the appendageal route are better compared to the area without them. This aspect is mostly interested in drug delivery over the skin as the hair follicle has a reservoir that naturally lies in the epidermal region [43]. Thus, there is a scope to utilise this natural pathway to extract and investigate ISF for further investigations. However, identifying the exact location of the hair follicle on different human subjects are still challenging. There are different platforms to extract and monitor ISF, including suction blister, iontophoresis, micro-dialysis, sonophoretic extraction, and MN array patches [44-46]. Each of these platforms has its own advantages and limitations.

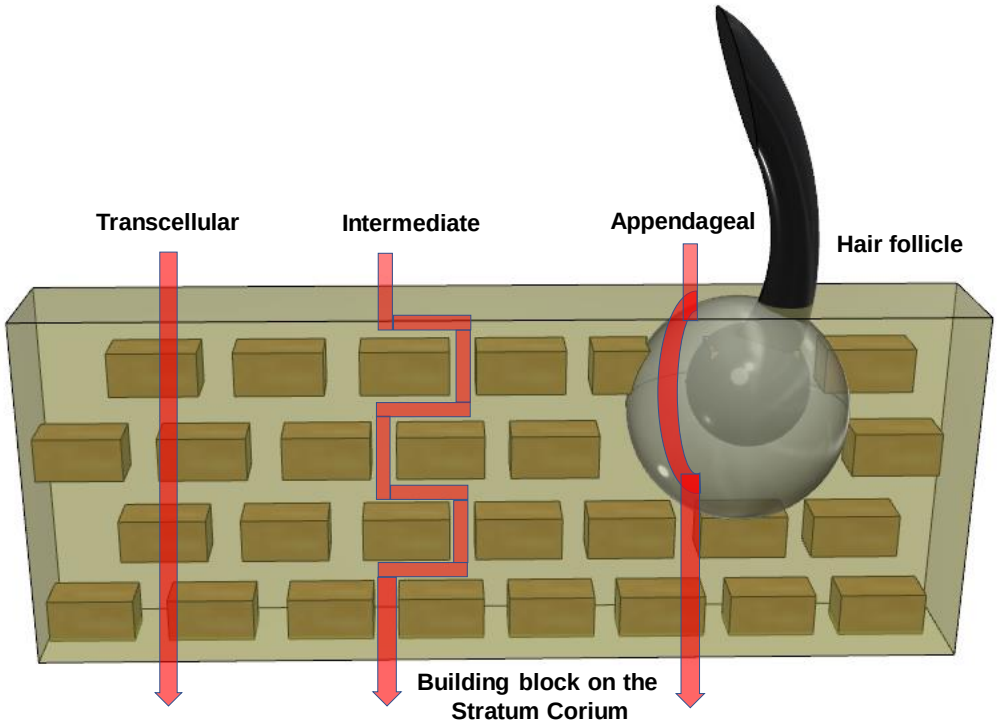

Figure 1. Schematic diagram of the human skin representing the three possible routes for the permeation of fluid substance. The path can be used for ISF sampling/extraction.

2.1 Suction blister

The suction blister was developed by Kiistala *et al.* to analyse the pathogenesis of blister formation during the separation of the epidermis from the dermis in human skin [47]. The model was later used to extract ISF from the skin. The technique involves the application of negative pressure (100-200 mmHg) with elevated temperature for long hours (60-90 min) in the skin. The applied pressure creates a blister between the dermis and epidermis. The dermal ISF filled the generated blister over time. The suction blister technique is widely used to investigate the wound healing property of the epidermis and skin disease treatment. However, this method is associated with severe injuries, infections, and bleeding in the skin, requiring weeks to heal. The absorbent of fluids by suction blister lacks quantitative tracking and needs a higher sample volume [48]. Yu *et al*. demonstrated ISF extraction through a micro-vacuum generator in a microfluidic system [49]. The target pig skin was pre-treated to augment the porosity with low-frequency ultrasound prior to the extraction. A micro pneumatic valve controlled the flow in the microchamber. A flow sensor was utilised for the volume measurements of the extracted ISF.

2.2 Iontophoresis

Iontophoresis uses an electrical charge on the skin surface to increase the ISF flow. The applied charge induces the electroosmotic solvent to flow from the anode to cathode connections [50]. Glucowatch was a commercially available product that utilised iontophoresis to continuously monitor glucose levels via integrated biosensors. However, the

Preprints (www.preprints.org) | NOT PEER-REVIEWED | Posted: 30 March 2021 doi:10.20944/preprints202103.0720.v1

report showed skin irritation for the continuous application, and a high false-positive rate was associated with the system. The product was eventually withdrawn from the markets. Kim *et al*. showed a needle-free device with reversed iontophoresis. They also compared their model with classical glucose monitoring (CGM) devices incorporating a needle [14]. The system analysed sweat stimulation at an anode (glucose oxidase biosensors), and ISF extraction at a cathode (alcohol oxidase biosensors) simultaneously in a wearable epidermal platform. The performance was evaluated by consuming food and alcohol to observe the change in sweat-alcohol and ISF-glucose in human subjects, respectively. The result showed a good and reliable glucose level in the ISF with a few minute delays. However, the system induced skin injuries during repetitive usage. Kim *et al*. demonstrated a screen-printed electrochemical path that used the iontophoretic extraction of ISF [51]. The panda-looking tattoo patches incorporated flexible electronics and worked as a stimulating sensor. The real-time performance detected reliable changes in glucose levels while consuming food and alcohol. However, the effects of iontophoretic extraction were not investigated for long term usage.

2.3 Sonophoresis

Sonophoresis uses low-frequency ultrasound in the skin. The ultrasound induces a cavity bubble that increases the skin's porosity. When vacuum pressure is combined with the ultrasound, the permeability of the skin augments by many folds. The result shows promising non-invasive extraction off ISF within 5-15 minutes. Ultrasound pre-treatment applied on the skin can persist the increased porosity for up to 42 hours under occlusion [52]. However, the approach is limited to extract ISF from shallow regions of the skin (epidermis) [53]. Pu *et al*. demonstrated CGM devices consisting of three electrodes attached in a microfluidic chip [54]. Ultrasound was utilised to increase the permeability of the skin. The microfluidic system used vacuum pressure to extract and collect the ISF of up to 1 μL. The working electrode was activated to sense the glucose response by a layer of graphene and gold nanoparticles (AuNPs). This composite nanostructure significantly improved the sensitivity of the system.

Soto *et al*. devised a flexible transdermal tattoo path with micro-ballistic pores to augment skin penetration by ultrasound triggering [55]. The patch contained thousands of micro-doses loaded with perfluorocarbon emulsion. The process drastically enhanced the permeability of the skin. Desired drugs were injected, and ISF was extracted without any complications. However, an external piezoelectric traducer was required to induce the ultrasound pulse. The pulse generated a pressure gradient between the patch and the skin. Mitragotri *et al*. showed the extraction of ISF from the skin by a combination of ultrasonic pulse and vacuum pressure [56]. The combination showed a drastic increase in skin permeabilities. The extracted ISF was analysed for the glucose concentration that correlated well with the blood glucose level.

2.4 Microdialysis

Microdialysis is relatively a mature method for sampling ISF for long-term continuous glucose monitoring [57]. Microdialysis uses an implantable probe normally made of semipermeable hollow fiber [58]. Perfusate solution is flown at a low flow rate of 0.5-5 μL/min that generates a concentration gradient in the dermal region. The sampling technique involves passive diffusion of a substance through a semipermeable membrane. The process can analyse the molecular weight of the analyte without changing the concentration of protein [59]. However, fine-tuning and frequent calibration is needed to maintain the sensitivity of the probe. The method is complex and external pumps are often required to supply the liquid.

Furthermore, the insertion of the sensor in a human subject involves a critical design challenge. Safety and toxicity are also major concerns for the implantation of the probe. Besides, sensor fouling is a common issue for long term observations. Sometimes, low-frequency ultrasound (1-3 MHz) is combined to increase the permeability of the skin prior to the implantation of the probe. This improves the performance of the microdialysis.

Preprints (www.preprints.org) | NOT PEER-REVIEWED | Posted: 30 March 2021 doi:10.20944/preprints202103.0720.v1

When designing the extraction technique of ISF, it is imperative to avoid local trauma to the skin area. Otherwise, the ISF composition may be contaminated with blood plasma, thus becoming difficult to analyse [60].

4.5 Microneedles

MNs with a length between 300-1500 μm can penetrate the dermal layer and collect ISF from the skin. Based on the geometry, MNs can be hollow, porous, solid, or hydrogel-based. Several factors need to be considered when using the MNs for extracting ISF. The major consideration is its geometry including length, diameter, size and shape, material selection considering biocompatibilities, and dimensions of the array. The MNs can be used as a probe for biosensing as well as collecting the fluids [61]. Solid MNs are associated with an integrated electrode or biosensor for sensing of ISF. The electrode layer incorporates conductive material such as gold, platinum, or silver. The biosensing layer uses enzymatic reactions to detect biomarkers such as glucose, proteins, and ions. The hollow and porous MNs uses capillary force for the extraction of ISF. However, fabrication of the hollow MNs is complex and costly compared to the solid and porous MNs. The porous or hollow MNs can be filled with suitable solutions to elevate ionic strength. This generates a pressure gradient between the MNs and the skin to increase the flow of ISF. As long as the pressure gradient is present, ISF flows through the micropores.

Wang *et al*. utilised 700-1500 μm long solid glass MNs to penetrate the skin [62]. ISF was extracted from the introduced pores with vacuum pressure. 1-10 μL of ISF was extracted within 2-10 minutes for glucose measurements. Mukerjee *et al*. pioneered the extraction of ISF utilising 250-350 μm long hollow MNs made off single crystal silicon using micromachining technique [63]. The extracted ISF was transferred to the backside of the microfluid system. A commercial glucose strip was used to investigate the concentration of glucose from the collected ISF. However, measurement delay was associated as the ISF diffused through the hollow space and reached the sensing compartments [64].

Porous MNs can either incorporate integrated sensors for on-spot analysis or investigate a part of the ISF through diffusion. Hydrogel MNs are normally dissolved into the skin, enabling the diffusion of the drug when contacting with the ISF. However, this process is time-consuming, and bulky instruments are required to recover the target biomarkers from the extracted ISF. This is due to the characteristics of the hydrogel, retaining a high level of water inside the structure. However, a recent report by He *et al*. suggests that hydrogel MNs fabricated by a combination of polyvinyl alcohol (PVA) and chitosan (CS) patch can avoid such issues [65]. The composite PVA/CS MNs were stiff when dry due to the phase transition properties. This allowed the MNs to penetrate the skin easily. Meanwhile, the thermal degradation property of the PVA provided an easy recovery of the target biomarkers from the MNs arrays.

Zheng *et al*. demonstrated faster extraction of ISF (3 folds) comparing with the existing platform. The team devised an osmolyte powered patch of 100 MNs array [66]. The MNs array was fabricated by a composition of osmolytes (maltose) and hydrogel (methacrylated hyaluronic acid) materials. The developed MNs patch extracted 7.9 μL and 3.83 μL of ISF from the pig and mouse skin *in vivo* within 3 mins, respectively.

3. Design considerations of MNs

There are generally four design considerations that need to be considered before designing an MN for biosensing applications **[67]**: 1) The sharpness of the needle that penetrates the skin; 2) Mechanical strength against bending, fracture and buckling; 3) Biocompatibility of the MNs; 4) Manufacturing consideration to meet the clinical requirements. Also, when designing an array of the MNs, it is important to consider the arrangement of the MNs arrays as well as the skin application manner (i.e., application by hand or by an applicator). The first two considerations, i.e., sharpness and strength, depends on the mechanical design considerations and will be explained in the next section. The biocompatibility will also be thoroughly discussed in Section 3.2. The fourth requirement is directly related to the fabrication procedures and is an essential factor that needs to be considered, especially for the commercialisation of the MNs.

Preprints (www.preprints.org) | NOT PEER-REVIEWED | Posted: 30 March 2021 doi:10.20944/preprints202103.0720.v1

3.1 Mechanical design

In designing MNs, three important forces need to be considered: (i) Insertion force, $\boldsymbol{F_{ins}}$; (ii) Buckling force, $\boldsymbol{F_{buck}}$ and (iii) Fracture force, $\boldsymbol{F_{fr}}$. Upon the insertion of the MNs, there is a significant risk that MNs fracture and remain inside the human's skin. To prevent this risk, the following relationship between these three forces need to be considered **[67]**:

$$F_{ins,max} < F_{buck} \ll F_{fr}, \tag{3}$$

$\boldsymbol{F_{ins,max}}$ is the maximum insertion force that depends on the MN tip diameter that determines the surface of the affected skin area, $\boldsymbol{A_s}$, initial force, $\boldsymbol{F_0}$, skin's puncture toughness, G_P, and characteristic insertion length, $\boldsymbol{\lambda}$. Accordingly, this force can be calculated as follows **[67]**:

$$F_{ins,max} = F_0 + \frac{1}{\lambda} G_P A, \tag{4}$$

Buckling force is calculated based on the Euler's critical load, as shown in Eq. 5:

$$F_{buck} = \frac{\pi^2}{4\,L^2} E I_A, \tag{5}$$

where E is Young's modulus of the MN material, I_A is the minimum area moment of inertia of the cross-section of the MN, and L is the total length of the MN.

Finally, the critical fracture force can be estimated using Eq. 6 **[67]**:

$$F_{fr} = \pi D \sin\alpha\, w_t\, \sigma_{cr}, \tag{6}$$

In this equation, D is the diameter of the needle tip, α is wall angle of the MN, w_t is MN's wall thickness and σ_{cr} is the critical stress of the MN's material.

An important design parameter is the MN's margin of safety, $\boldsymbol{\psi}$, which is the ratio of the critical fracture force to the maximum insertion force **[68]**. Considering Eqs. 4 & 6, this parameter can be calculated as follows:

$$\psi = \frac{\pi D \sin\alpha\, w_t\, \sigma_{cr}}{F_0 + \frac{1}{\lambda} G_P A}, \tag{7}$$

To assure the safety of a MN, the MN's margin of safety should be much larger than unity. Eq. 7 illustrates how the geometrical parameters of a MN can be tuned to increase the MN's margin of safety. For instance, as the equation suggests, by expanding the MN's wall thickness and/or decreasing the needle tip, the values of ψ can be increased.

3.2 Biocompatibility analysis

One of the important components needing attention in designing any MN devices is the biocompatibility of both the material and the reagents used. Although these devices appear to be on the body's surface, they do also breach the skin barrier. This breach can cause acute changes to the structure of the skin and cause vascular damages. Vascular damages have the potential to provide space for blood contamination. For an MN device, two different biocompatibility assessments must be satisfied: (i) surface device – skin contact and (ii) surface device – skin breaching. Biocompatibility tests are usually performed following the ISO 10993 regulations [69]. The regulation recommends the evaluation of both systemic and local reactions. Furthermore, it also recommends long term systemic toxicity studies for the entire biological system, such as the nervous system or immune system.

Over the past few years, numerous studies have been conducted to analyse the biocompatibility of materials for MNs. Wu *et al.* reported investigation on drug delivery by intradermal MN system. The extraction of silicon MN was prepared by immersing the material in physiological saline at 37°C for 72 hrs with a proportion of 3 cm^2 of material per mL. The evaluation was done by bone marrow micronucleus test in mice, Ames test on four types of *S. typhimurium* strains, *in vitro* cytotoxicity test, *in vitro* mammalian cell gene mutation test, the maximisation test and the primary skin irritation test on New Zealand white rabbits. Also, the maximisation test was performed to assess the primary skin irritation [70]. Recently, Schossleitner *et al.* investigated the biocompatibility of MNs from

Preprints (www.preprints.org) | NOT PEER-REVIEWED | Posted: 30 March 2021 doi:10.20944/preprints202103.0720.v1

cyclic olefin polymer [71]. In this study, epithelial and human endothelial cells were used for testing with the elution method and the direct contact method. The evaluations were done on the basis of cell viability, morphology, cellular differential and barrier formation. The team also used inflammatory markers such as E-Selectin and ICAM-1 to assess immune cell adhesion potential [71]. Moussi et al. conducted the cytotoxicity analysis to determine the biocompatibility of 3D printed MNs [72]. The test results were evaluated by cell viability in direct contact with the material and the material extract for different time frame [72].

Although different researchers used different methods for biocompatibility analysis, the most systematic approaches for evaluating biocompatibility of MNs are (i) *in vitro* tests (ii) *in vivo* tests, and (iii) Clinical trials (Figure 2) [73,74]. As the name suggests, the *in vitro* tests are performed outside living organisms, mostly in a cell culture-based platform. Individual components used for the production are individually co-cultured with the cells for any biological response. For flat surfaces like PDMS (polydimethylsiloxane) or PMMA (polymethyl methacrylate) membranes, cells can be cultured over these surfaces to note the response [75,76]. The most common biological responses recorded are cell death, cell lysis, inhibition of cell growth and morphological changes [77]. During this initial phase of testing, not only the materials but any eluate or extracts are also tested for effects in the cells. Different methods are available to evaluate the cells' response when they come in contact with the material or their eluate/extracts. One common method is to test the leak of an enzyme like LDH from the cells [78]. Another approach is testing the permeability of the membrane with membrane-impermeable dyes. For MNs devices, their potential to come in contact with blood cells is high due to skin breaching. In these situations, it is also recommended to perform hemocompatibility analyses. The most common form of hemocompatibility analysis is looking for potential hemolysis after incubation of blood cells with the test material. The amount of hemoglobin released from the cells is quantified. Extensive tests such as partial thromboplastin time test and complement activation test are also recommended to evaluate any adverse effect of the MNs in blood coagulation [79].

The *in vivo* tests are performed by applying the MNs to the test animals, usually mice. Unlike the *in vitro* assays, the final device is tested and not the individual components. These assays are typically performed after the MNs are determined biocompatible from the *in vitro* assays. The most common assay for the MN arrays is their hemocompatibility, looking into the thrombogenic potential. Any activation of platelets, formation of thrombi or emboli or cellular injury is reported. For MNs, additional *in vitro* assays like testing the dermal irritation or the Murine Local Lymph Node Assay (LLNA) is also recommended [80]. Dermal irritation assay is usually qualitative and is weak in demonstrating the response to MNs, whereas LLNA is more reliable and widely accepted method to determine the skin sensitising potential. Alternative to the murine model for this assay is a guinea pig animal model. Some *Ex vivo* models are also developed to minimise the effects on the *in vivo* animal models. These models however lack the whole immune response and only present the opportunity to study local effects. Moreover, these *Ex vivo* models are not yet recommended by the ISO guidelines.

The most relevant test for combability assessment is the clinical trials itself. MNs device applied to a human volunteer would give the best results in terms of safety and efficacy. Nevertheless, it is more expensive, more difficult to control and legally complex. Therefore, this process is usually followed after successful MN's *in vitro* testing of materials and *In vivo* models testing. Although successful *in vitro* or *in vivo* testing does not guarantee clinical trials success, many examples of devices are redesigned after entering the clinical trial phase. However, there is a consensus that cytotoxicity, hemotoxicity testing of every MN device components on *in vitro* models is necessary. Extended hemotoxicity assays, irritability testing, and any systemic response is tested with the *In vivo* models before proceeding to clinical trials.

Preprints (www.preprints.org) | NOT PEER-REVIEWED | Posted: 30 March 2021 doi:10.20944/preprints202103.0720.v1

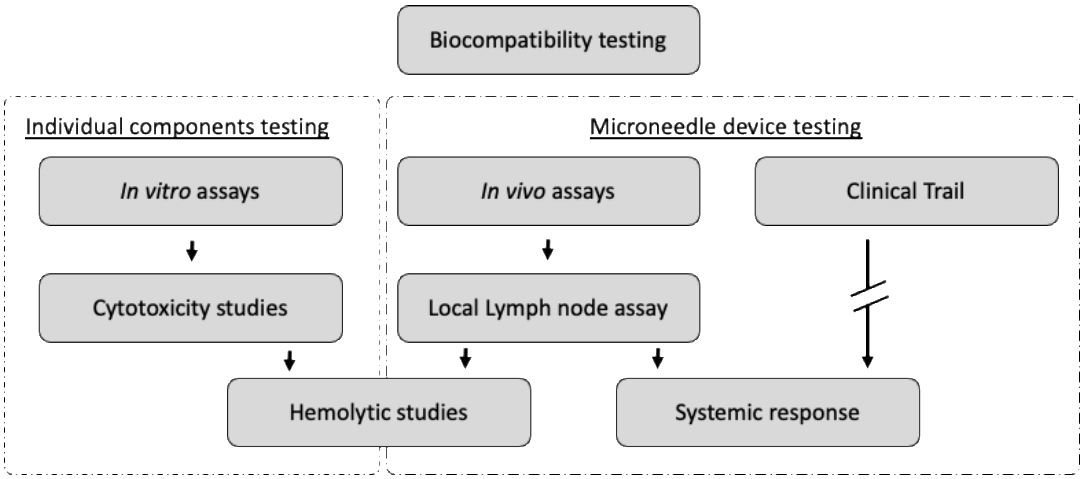

Figure 2. Schematic diagram showing the biocompatibility assessment process. Individual components of the MNs are tested for cytotoxicity or hemotoxicity by *in vitro* assays. In vivo assays test the whole device for any systemic responses and LLNA in addition to the hemocompatibility assays. The final stage of testing is the clinical trial, where all the reactions and toxicity are studied before accepting the MN device for general use.

4. Fabrication of Microneedles

The cutting-edge advances in microfabrication can revolutionise the way MNs are made. In the literature, a wide variety of microfabrication techniques have been used to produce MNs for ISF sampling and sensing [81]. Four common types of MNs can be used for ISF sensing and sampling: solid MNs, hollow MNs, porous MNs, and hydrogel MNs. Figure 3 shows images of some of these MNs fabricated by different techniques. In this section, these fabrication techniques are discussed base on the above four categories.

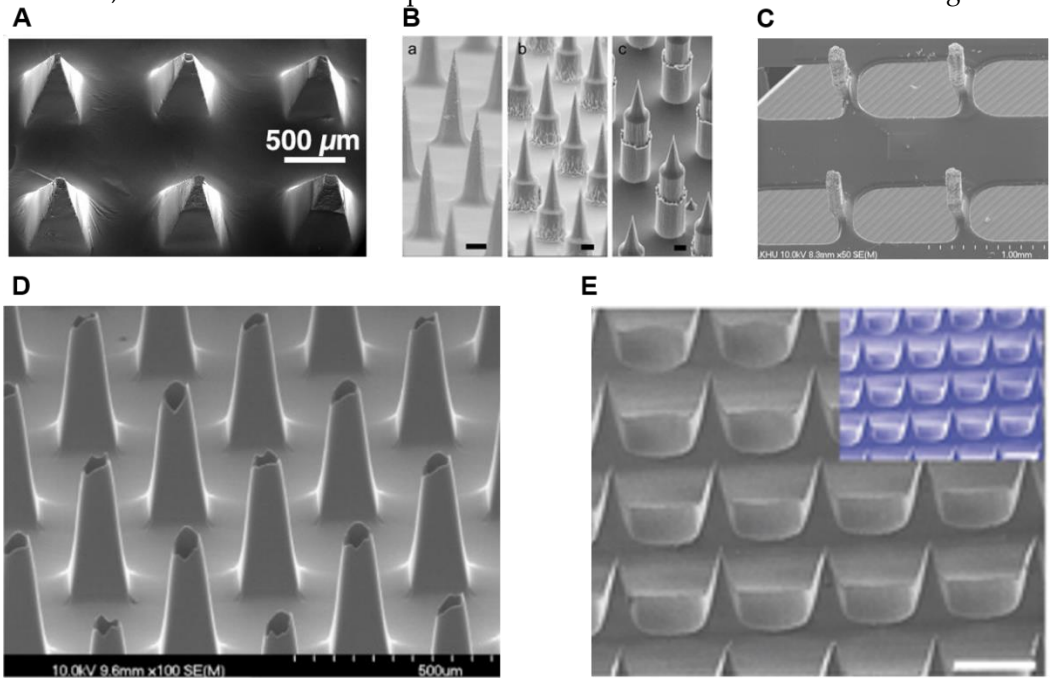

Figure 3. SEM images of solid, hollow, and hydrogel MNs fabricated by different techniques. A) Solid MNs fabricated through injection moulding [83]. B) Solid MNs made via deep reactive ion etching (DRIE) with various tip profiles: a) tapered tip; b) tapered tip plus short Bosch etch; c) tapered tip plus longer Bosch etch. The scale bar = 10 μm. [84]. C) Solid MNs produced via wet chemical etchant [85]. D) Hollow MNs produced by DRIE and plasma etching [87], E) Hydrogel MNs fabricated by casting method. The scale bar is 500 μm [90]. The figures have been reproduced with permissions from Refs. [83], [84], [85], [87] and [90], respectively.

Preprints (www.preprints.org) | NOT PEER-REVIEWED | Posted: 30 March 2021 doi:10.20944/preprints202103.0720.v1

4.1 Solid MNs

Solid MNs were generally functionalised to serve as bio-electrodes and sometimes to punch the skin [91]. The fabrication techniques that were reported for producing solid MNs are 1) casting [82,92-101]; 2) injection moulding [83,102-107], Figure 3A; 3) DRIE [84,108-110], Figure 3B, and 4) wet chemical etchant [85,111], Figure 3C. Solid MNs for ISF sampling were also fabricated using infrared laser [112] and lithographically defined chemical etching [113].

Figure 4A-D demonstrates the process and basic principle of the most common fabrication techniques of the ISF solid MNs schematically as well as MNs surface modification steps. These methods will be briefly introduced in the following sections.

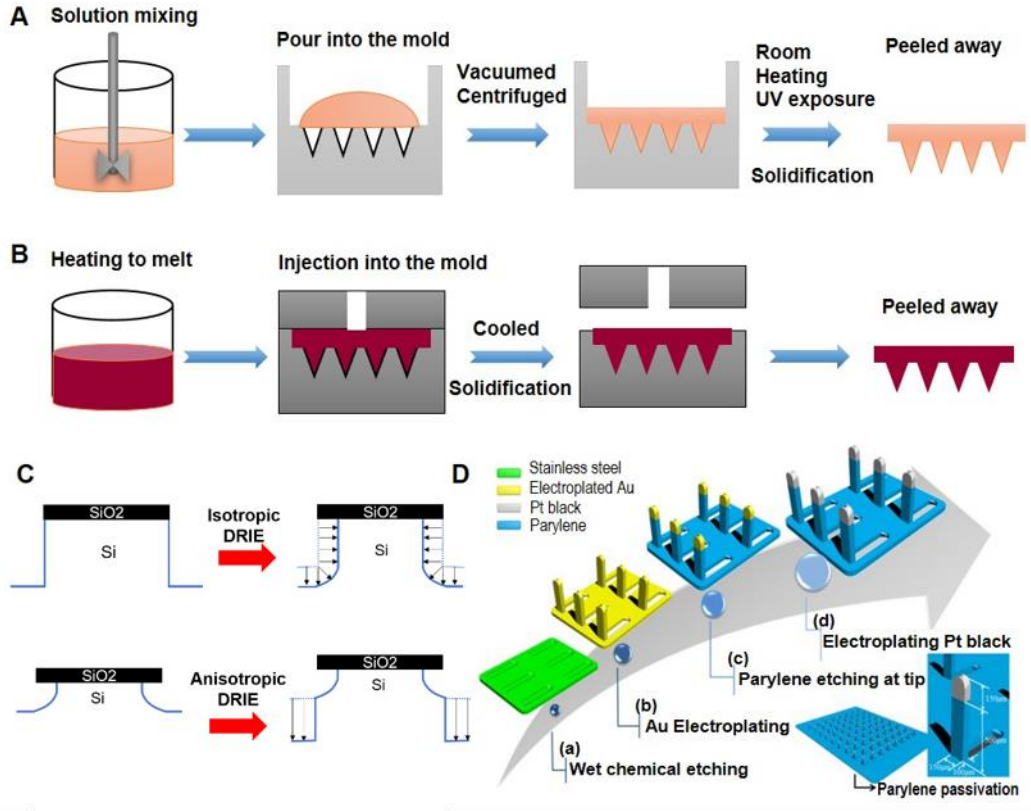

Figure 4. Fabrication processes of MNs. A) The casting method includes preparing a solution mixture, pouring the solution mixture into the mould, vacuumed or centrifuging to completely fill the mould, leaving at room temperature, heating or UV exposure for solidification, and then peel away the prepared MNs. B) Injection moulding that includes heating the sample to melt, injection into the mould, cooling to solidification, and then peel away the prepared MNs. C) Basic processing principle in deep reactive ion etching (DRIE) (a) Isotropic plasma etch of MNs vertical walls in DRIE etched with high aspect ratio in a silicon substrate, (b) Anisotropic plasma etch of the silicon dioxide mask, and (c) Principle of the basic process for producing high aspect ratio structures in DRIE technology [114]. The figure was redrawn with some changes from Ref. [114]. D) Wet chemical etchant, steps of solid MNs fabrication that was surface modified with Pt black catalytic layer for a non-enzymatic glucose sensor, a) wet chemical etching in stainless steel substrate, b) Au electroplating, c) Parylene etching at the tip, and d) electroplating for Pt black [85]. The figure was reproduced with permission (with some changes in the text of the original figure) from Ref. [85].

4.1.1 Casting Method

The vast majority of solid MNs was created through casting micro-moulding techniques using a prefabricated mould. The required steps are schematically shown in Figure 4A. In the casting manufacturing process, a liquid material is usually poured into a mould that contains hollow cavities with the desired template. The sample is allowed to solidify under ambient condition by UV light exposure or by baking. In the micro-casting process, the sample is usually placed in a vacuum or centrifuged to release air and draw the

Preprints (www.preprints.org) | NOT PEER-REVIEWED | Posted: 30 March 2021 doi:10.20944/preprints202103.0720.v1

homogenous solution to the cavities' tips to create a sharp tip. The solidified part is ejected or broken out of the template to complete the process. Prefabricated silicon moulds were frequently used for MNs fabrication in casting technique. Micromachined silicon parts were also used to create female/male PDMS mould to obtain flexible mould through the casting method [94].

Solid MNs made of sodium chondroitin sulfate through the casting on a prefabricated mould were inserted into the skin and then removed to create pores for ISF extraction [92]. Composite MNs were made with a solution of palladium nanoclusters combined with polystyrene beads in cyclohexanone prepared by casting into a silicone mould, and applied for electrocatalytic detection of peroxide [82]. Another work reported nanocarbon–cellulose acetate phthalate composition to fabricate electrochemically controlled dissolution MN arrays for pH measurement [93]. The MNs were created via casting a mixture of dispersed nanocarbon within the polymer and dissolved in cyclohexanone. Polymeric MNs loaded with photonic crystal barcodes fabricated by the ferrofluid casting method was used for biomarkers detection [100]. Senel et al. casted gold ink (Au nanoparticles and organic polymer) onto a PDMS mould [101]. The fabricated gold MNs was functionalised with a urease enzyme for urea sensing. Norland optical adhesive (NOA) was poured into the PDMS mould, cured with UV light to construct on-chip MNs electrodes for glucose detection [94]. The electrodes were gold coated and then covered with a thin layer of NOA polymer. The sample was heated to reduce the NOA's viscosity and flow down away from the MNs tips to have gold tips. The device then was covered with platinum and finally modified with sulphonated-β-cyclodextrin. In another work, NOA MNs were functionalised with plasmonically active gold nanorods and covered with the pH-sensitive molecule 4-mercaptobenzoic acid to use in Surface Enhanced Raman Spectroscopy (SERS) [95]. SERS was implemented with PMMA MN coated by silver nanoparticles and functionalised with 1-decanethiol [96]. The PMMA MN array was prepared using a stainless-steel master mould.

Two works reported hydrogel coating for solid MNs [97,98]. In these studies, hydrogel-coating swelled upon skin insertion and formed a porous matrix to leukocyte uptake. Figure 4A illustrates the coating procedure. Solid MNs were generated by casting melted Poly-L-lactide over the PDMS mould [97]. In the other work, bare hydrogel-coated MNs was functionalised with an alginate–peptide nucleic acid mixture for sensing specific circulating nucleic acids [98]. The MNs arranged into three arrays were applied as working, counter and reference electrodes in a continuous glucose monitoring device [99]. The MN arrays were produced by casting the SU-8 photoresist polymer into a master mould and then exposed to UV light for solidification. The sample was treated with immiscible enzyme-mediator compounds of glucose oxidase enzyme and tetrathiafulvalene mediator through a spray aerosol mixing technique. The casting method is the most straightforward and low-cost microfabrication method frequently used in MNs production. This technique does not need expensive and high-tech instruments. In this method, MNs of various designs and dimensions can be prepared and easily scaled up. However, to have a sharp tip and completely filled corner, the sample needs to be centrifuged or vacuumed.

4.1.2 Injection moulding

A significant number of ISF sensing studies applied a platform with four arrays of MNs in a unique substrate [83,102-107]. In injection moulding, molten materials are injected into a mould by heat, then cooled and solidified., Figure 4B. For MNs arrays, the mould is created from substrates of copper–tungsten or stainless steel by an electric discharge milling. The samples were made with polycarbonate. The metal mould was used as electrodes for aluminium blocks spark erosion [102]. In these studies, MNs arrays with surface modification were utilised as electrodes. Three arrays of MNs were used as the working electrodes, and one MNs array was used as a reference electrode. The surface of MNs arrays was modified and functionalised differently for the intended applications. The working electrodes were metalised with chromium/platinum, and the reference electrode was sputtered with Ag, followed by iridium oxide deposition. The sample was then fixed with a beta-lactamase enzyme within a hydrogel for sensing beta-lactam antibiotic

Preprints (www.preprints.org) | NOT PEER-REVIEWED | Posted: 30 March 2021 doi:10.20944/preprints202103.0720.v1

[103]. The array was also electropolymerised with polyphenols for evaluating theophylline [104]. In other work, three electrodes were coated with gold (as a working electrode), and the fourth electrode was coated with silver (as a reference electrode). The surface of the gold electrodes was electrodeposited by multi-walled carbon nanotubes, then electropolymerised with the redox mediator, methylene blue, followed by lactate oxidase enzyme through drop-casting to capture electron transfer of lactate oxidase [105]. In two other studies, the silver coated electrode was chloritized and applied as a silver–silver chloride reference electrode. The working electrodes were electrodeposited by iridium oxide to pH measurement. The sample was finally treated with a hydrogel layer containing an extended-spectrum βlactamase to monitor phenoxymethylpenicillin in healthy human volunteers [106] and detection β-Lactam antibiotic concentrations [83]. In one study, the gold coated electrode was electrodeposited with highly porous gold by cycling the potential in a solution of $HAuCl_3$ and NH_4Cl. The surface of the MNs was then modified by 6-(ferrocenyl) hexanethiol and adenine dinucleotide glucose dehydrogenase enzyme for glucose detection [107]. Injection moulding is a low-cost, mass production manufacturing technique commonly used for polycarbonate MNs production. The method is not suitable for the fabrication of preloaded sensing materials because they will be melted during the manufacturing process. High temperatures reduce and/or diminish the biomarker effectiveness.

4.1.3 Deep reactive ion etching (DRIE)

Researchers created MNs using deep reactive-ion etching (DRIE) technique [84,108-110]. In DRIE, structures with high aspect ratios are produced by applying a highly anisotropic etching process. This procedure is illustrated in Figure 4C. Using DRIE, deep penetration, steep-sided holes, and cavities can be constructed. To start with, a SU-8 photoresist was first deposited onto a silicon wafer. Next, the wafer was plasma etched to create the needle tip. The height of the MNs was developed via a standard Bosch process. The residual SU-8 was removed by oxygen plasma. After that, a silicon oxide layer was expanded using a dry oxygen furnace. The residual oxide was cleaned by acid etching, and sharpened silicon projections were produced [84]. DRIE fabricated MNs were surface modified with chrome and gold sputtering and functionalised with poly(ethylene glycol) to detect circulating biomarker [108-110]. The most significant advantage of DRIE is producing deep penetration and steep-sided holes with high aspect ratio. However, DRIE requires complex and expensive instruments as well as cleanroom facilities with unique treatments and complicated, time-consuming processes.

4.1.4 Wet chemical etchant

Wet chemical etching (WCE) was also reported for MN fabrication [85,111]. In wet etching, patterns are created on a base substrate by removing materials using liquid chemicals. A mask is used to draw the desired patterns on the substrate. During the etching process, materials that are not protected by the mask were washed away. These steps are schematically shown in Figure 4D.

Researchers applied a jet of ferric chloride in WCE to produce MNs electrodes [85,111]. The structure was patterned on stainless steel under pressure. The needles were then cut-out and bend 90◦ by a jig. The sample was electroplated with a thin layer of gold and followed by a Parylene coating. Dry-etched was done on the selected tips to form the Pt black layer by electroplated lead acetate, hydrochloric acid, and platinic acid onto the surface. Finally, the MN was dip-coated with a mixture of ethanol and Nafion, and was used for glucose monitoring in an enzyme-free biosensor [85]. Another study produced stainless steel MNs with the same procedure and coated Pt black with a solution of chloroplatinic acid, lead acetate and HCL [111]. In wet etching, the produced MNs have a uniform thickness in one dimension. However, the fabrication of tapered and pyramidal MNs cannot be done using that technique. Additionally, this method cannot be used to produce sharp tip MNs. In the wet etching process, the dissolution of the protected mask also must be considered.

Solid MNs fabricated by infrared laser [112], and lithographically defined chemical etching [113] were integrated with Whatman filter paper for biomarker and drug (polio-

Preprints (www.preprints.org) | NOT PEER-REVIEWED | Posted: 30 March 2021 doi:10.20944/preprints202103.0720.v1

specific neutralising antibodies and anti-polio IgG) monitoring in ISF. The pattern of the MNs was created on a stainless-steel sheet and then cut by an infrared laser. The sample was electropolished and cleaned with isopropyl alcohol and DI water and dried with air. It was plasma treated and Parylene coated to create a hydrophobic surface for ISF absorption [112]. The lithography technique is explained in Section 4.2.1.

4.2 Hollow MNs

Hollow MNs were used to extract and collect ISF out of body or their lumen functionalised to act as the biosensor or their hollow is filled with metal and metal-based material to act as bio-electrodes. The reported fabrication technique for hollow MNs are combined methods, including standard photolithography and etching [86,88,115-117], DRIE and plasma etching [87,114,118-121], and casting and plasma etching [88,122,123]. They were also fabricated using CO_2 laser machining [124], injection moulding [125], 3D printing [126], CNC-micromachining technique [127].

4.2.1 Standard photolithography and etching

Several works reported combined manufacturing processes, including standard photolithography, etching and DRIE for hollow MNs fabrication [86,88,115]. In photolithography, a thick layer of photoresist was spin-coated on a wafer. The wafer was then soft-baked and exposed to UV light through a dark-field mask containing desired arrays. The sample was immersed in a developer solution to remove the unexposed photoresist and then was hard-baked at elevated temperature. The pillars are formed at the end of the process [88]. First, one side of the silicon wafer is thermally oxidised. Next, parallel microchannels were produced using standard photolithography and etching. Microholes were created from a photoresist and then etched by DRIE. In the same manner, holes on the opposite side of the wafer were produced. The holes on the opposite side were connected to each other using DRIE. Then the wafer surface was coated with silicon nitride and subsequently bonded to a borosilicate glass wafer. After that, an automatic wafer dicing saw was applied to build silicon columns. The columns were aligned to off-centre holes near one corner. Finally, an aqueous solution was used to sharpen the MNs [88].

Polymeric hollow MNs were also fabricated from Eshell 200 acrylate-based polymer through polymerisation using a UV rapid prototyping system [116,117]. To this aim, a 3D computer model was applied to guide the light of a halogen bulb over a photosensitive material to polymerise the selectively exposed area. The sample was then washed in a proper solvent to remove the non-polymerised material, and then cured. The lumen of MNs was loaded with a mixture of rhodium and carbon dispersed in lactate oxidase to construct an amperometric sensor [116]. Miller *et al.* integrated carbon fibre electrodes within the polymeric hollow MNs for electrochemical sensing [117].

Photolithography and etching techniques produce the most similar MNs compared to the intended design. However, these techniques have limitations in creating high-aspect-ratio MNs because of the lithography substrate projection restrictions. These methods include complicated multi-step processes and require several trial-error steps and long fabrication time. Moreover, this technique needs expensive, special devices and cleanroom facilities, making it hard to be accessible in every lab.

4.2.2 DRIE and plasma etching

The hollow MNs was also etched onto a silicon wafer using DRIE while the needle tip was sharpened via an HNA (hydrofluoric acid-nitric acid-acetic acid) etching [87]. In one study, the hollow silicon MNs were connected to an amperometric glucose sensor [118]. In another study, the hollow silicon MN's inner lumen was modified by the metal electrodeposition process (gold-nickel-gold electrodeposition) and used as a micro-reactor for real-time detection without the need for sample transfer [119]. Another single out-of-plane hollow metallic MN was integrated with photonic components to incorporate enzyme-linked assays [120]. The inner lumen surface of the MN was functionalised to capture the target component. Griss *et al.* created sharp-tip and side-opening hollow MNs

Preprints (www.preprints.org) | NOT PEER-REVIEWED | Posted: 30 March 2021 doi:10.20944/preprints202103.0720.v1

using two-mask process by an inductively coupled plasma (ICP) system appalling anisotropic DRIE through the Bosch process and isotropic plasma etching [114]. The needles tip was sharpened by wet oxidation and a consecutive oxide strip. The produced hollow MNs were then applied for continuous glucose monitoring [121]. The ability to create high aspect ratio cavities and holes makes DRIE a good candidate for hollow MNs fabrication. However, DRIE has some challenges that were discussed in Section 4.1.3.

4.2.3 Casting and plasma etching

Mansoor *et al.* used solid SU-8 MNs to fabricate polymeric hollow MNs using combined casting and plasma etching technique [88]. First, a conductive polymer composite of PMMA seeded with carbon black (CB), in *N*-methyl-2-pyrrolidone (NMP)) was cast into the SU-8 master mould and then plasma etched with O_2-CF_4. The sample was metal (nickel) electrodeposited. Next, the conductive polymer composite was dissolved to prepare the open-tip MN array. In the final step, the surface of MNs was coated with a thin layer of gold. Master mould was created by the lithography method [88]. A sampling device with an MN was manufactured via polymerised silicone, cast into a 3D-printed master mould [122]. A 30G hypodermic needle was used as a mould for MN fabrication. In the other work, a mixture of silk with D-sorbitol and glucose oxidase was cast into the PDMS mould. Then, enzyme coated metal wires were inserted into the mould and allowed to dry to produce electrochemical transducers for monitoring glucose continuously [123]. In contrast to the solid MNs, only a few articles reported the casting method for the hollow MNs fabrication. One of the reasons can be the difficulties and challenges of master mould production for hollow MNs. However, we anticipate advances in the near future.

4.2.4 Miscellaneous methods

Miscellaneous methods were also reported for hollow MNs fabrication, including CO_2 laser machining [124], injection moulding [125], 3D printing [126] and CNC-micromachining technique [127]. A hollow MN can be fabricated through CO_2 laser machining from PMMA, and integrated with a microfluidic chip for potassium sensing [124]. Mohan et al. fabricated polymer MNs via injection-moulding into a high-carbon stainless steel mould constructed by a computer numerical control (CNC) machine [125]. Then, enzyme coated metal wires (platinum and silver) were inserted into the lumen of the MNs. Recently, acrylate-based polymer hollow MNs were 3D printed and then treated with carbon and functionalised with a catechol-agar (phosphate-buffer) solution for skin melanoma screening [126]. CNC-micromachining technique was used to fabricate an array of four hollow MNs sensor for ketone bodies detection. An optimised mixture of enzyme/cofactor was cast onto the MN electrodes for biomolecules absorption [127]. Prefabricated ultrafine pen needles made of stainless steel was also used as hollow MNs. The needles were integrated with a 3D-printed holder to extraction and collection ISF [60,128].

4.3 Porous MNs

Porous materials have a large volume of pores to extract fluid by capillary force. Casting technique [61,89,129-132] and thermal drawing lithography [133] are two fabrication methods that were reported for porous MNs construction for ISF sampling. The porous structures were created via the leaching and sintering process. To date, there are only four reports in the literature that used porous MNs for ISF sampling.

4.3.1 Casting method

Using photo-polymerisation under UV light, Liu *et al.* created porous polymer MNs made of an acrylate monomer with a porogen [129]. The polymer mixture was cast into a negative PDMS mould, and the baked sample was leached in proper solution. The created porous MNs was then used for intercellular swelling monitoring [132]. Polyvinyl formal porous MNs was prepared from aqueous solutions of polyvinyl alcohol in water and starch, formaldehyde solution, n-pentane and sulfuric acid for ISF extraction [89]. Moreover, porous PDMS MNs was fabricated by casting a mixture of PDMS with salt into a PDMS mould followed by salt leaching [61,130]. PDMS is a soft and hydrophobic material. The porous PDMS MNs is not strong enough to penetrate the skin. To enhance the mechanical strength and to achieve a fluidic path of liquid inside the porous PDMS MNs, the

Preprints (www.preprints.org) | NOT PEER-REVIEWED | Posted: 30 March 2021 doi:10.20944/preprints202103.0720.v1

array was treated with hyaluronic acid (HA). The HA-supported porous PDMS MNs are strong enough to penetrate the aluminium foil and the agarose. The HA coating dissolved once contact to the water creating fluidic paths for MNs [61]. In the other work with pure porous PDMS MNs, a solid master mould was used to punch the simulated skin, then the MNs was inserted into the produced pores, and finger pressure was applied into the MNs for liquid extraction [130]. Ceramic materials have suitable mechanical properties for MNs. Porous ceramic MNs were fabricated with two slurry- and resin-based formulations via cast into PDMS mould under centrifugal force, followed by sintering at high temperatures [131]. The casting method is an easy and applicable method for porous MNs fabrication. The most challenging issue of porous MNs is the poor mechanical strength of the produced MNs to pierce the skin, which is related to the structure and material, not the fabrication method.

4.3.2 Thermal drawing lithography

Morishita *et al.* used thermal drawing lithography and salt-leaching method to fabricated porous MNs made with poly lactic-co-glycolic acid for ISF extraction [133]. Through the thermal drawing lithography method, the materials were heated on a base plate. A hot micropillar was lowered down and contact on the sample. The heating system then was quenched. MNs were generated by lift up the micropillar. The sample was let to be cooled, solidified and then was salt-leached. The thermal drawing lithography method is easy to perform. It does not need 3D mould fabrication. However, the produced MNs have not accurately the same size and dimension as the microfabricated MNs. High temperature in thermal drawing lithography limits heat-sensitive biomarker loading. On the other hand, in thermal drawing lithography, ultra-long solid MNs can be produced that can be applied as the master mould for hollow MNs fabrication.

4.4 Hydrogel MNs

Hydrogel are liquid-swollen materials that are good candidate for ISF extraction [66,90,134]. Hydrogel MNs swell by ISF absorption without dissolution in the skin [135,136]. The swelling degree of these MNs depends on the cross-linker content and crosslinking period [136]. Hydrogel MNs are generally fabricated by casting aqueous blends into the mould, and then crosslinked by heating or UV exposure. For example, hydrogel MNs were prepared from an aqueous mixture of hydrolysed poly (methyl-vinylether-co-maleic anhydride) and poly(ethyleneglycol) which was crosslinked by heating [135-138] and applied for lithium detection [138]. The other hydrogel MNs made of methacrylated hyaluronic acid [66,90], polyacrylamide [139], polyvinyl alcohol and chitosan [65], and gelatin methacryloyl [123,140] were reported for optical fluorescence sensing [139], cell-free DNA monitoring [141], glucose measurement [65] and urea sensing [140]. With respect to hydrogel properties, the casing method is the most appropriate fabrication method for hydrogel MNs. The details of the casting method were addressed in Section 4.3.1.

4.5 Challenges associated with microneedle fabrication

Generally, fabrication technology of solid MNs is more straightforward than that of hollow MNs. The geometry of the hollow MNs is complicated for producing due to the lumen holes. Their lumen needs high aspect ratio construction that makes the fabrication process challenging. Solid MNs can be produced by a particular standard lithography technique, DIRE, Wet etching, or plasma etching. Such methods require unique treatments with complicated, time-consuming processes. However, to produce hollow MNs, a combination of these techniques is needed. Such multi-step fabrication processes are more time-consuming and not suitable for mass production as compared to solid MNs. There are similar challenges in the casting method, which is originally a simple and low-cost fabrication technique compared to the other microfabrication methods. Although solid MNs can be fabricated easily using the casting method, hollow MNs need multi-step processes to prepare through the casting method. Besides, cast solid MNs have a more uniform and homogenous structure than hollow ones. Many researchers used injection

Preprints (www.preprints.org) | NOT PEER-REVIEWED | Posted: 30 March 2021 doi:10.20944/preprints202103.0720.v1

moulding for solid MNs fabrication, while this method is less popular for hollow MNs fabrication. Difficulties of the master mould manufacturing for hollow MNs with narrow lumen can be one of the reasons. The challenge of the master mould fabrication for the hollow MNs also exists for the casting method. However, most of the master moulds of the casting method are made of silicon using lithography. Such an approach is more straightforward than metal master mould fabrication for injection moulding. Production of the master mould for the casting method is similar to the fabrication of solid MNs with a high aspect ratio to produce the needle lumen. Some works used wires of metal or carbon pastes into the lumen of the hollow MNs to produce electrodes. However, these steps are done manually, which reduces the fabrication accuracy and makes the fabrication method not suitable for mass production.

In comparison, solid MNs with proper surface modification and metal coating are more suitable candidates to serve as microelectrodes. The structure of the hollow MNs makes their manufacturing process more complicated than the solid MNs; however, hollow MNs are a better choice for ISF extraction and sampling. For the porous and hydrogel MNs, the casing method is the most used and appropriate fabrication method.

5. Sensing mechanisms of ISF detection

As mentioned above, ISF forms the interface between cells and the blood capillaries. The composition and biophysical properties of ISF mainly depend upon the type of surrounding cells and are influenced by the physiological, developmental, or pathological state of the surrounding cells. Pathological alterations of the cells are reflected in the ISF [142]. Consequently, interest in utilising ISF for disease biomarker discovery or as a sample source for diagnostic applications has increased significantly in recent years. As a source of biomarkers, ISF offers several advantages compared to the most commonly used biofluid such as blood. For instance, plasma proteome is a highly complex mixture of proteins originating from various body cells, a large proportion of which may be completely unrelated to the disease condition. Identification of disease-specific biomarkers amongst such an overwhelmingly large number of unrelated molecules is a daunting task. Concentrations of disease-specific proteins in plasma may be 1-10 pg/mL, or even lower. The majority of ISF components, in contrast, are derived from cells in close vicinity; thus, disease-specific biomarkers are enriched compared to blood/plasma. For example, it has been shown that the concentration of tumour biomarkers can be 1000-1500 times more in the tumour microenvironment compared to blood [143]. Levels of high abundance proteins such as serum albumin and immunoglobulins are also remarkably lesser in ISF compared to plasma; thus, low abundance protein biomarkers are not masked. One other salient feature of ISF is that while 83% of serum proteins are also found in ISF, only 50% of ISF proteins are found in serum, indicating ISF contains a large number of unique biomarkers [41]. It can be inferred that what has been said about protein biomarkers in the preceding discussion may be equally valid for other potential biomarkers like DNA, miRNAs, even though very few relevant studies are available [144].

Since Celis and co-workers' pioneering work on proteomic profiling of tumour interstitial fluid [145], the molecular composition of ISF has been well characterised [48,146-148]. Several studies have explored the utility of ISF from various body organs as a source of disease biomarkers [142,146,149]. However, despite all these advantages, for most of the body organs, tissue interstitial fluid is hard to access and procedures involved may be even more invasive compared to venepuncture. Therefore, most of the studies related to biomolecular profiling in ISF focus primarily on discovery rather than translational and clinical applications. Although there are a number of interstitial regions, dermal and subcutaneous interstitial compartments are the most easily accessible, hence the interest for utilising ISF as a diagnostic fluid is largely limited to these compartments. However, extraction of dermal ISF using currently available techniques is not suited for routine clinical applications as it involves longer wait times and smaller sample volumes. Therefore, MN-based platforms that can provide continuous bioanalyte monitoring can prove to be potential candidates for clinical or patient self-monitoring applications. MNs-based

Preprints (www.preprints.org) | NOT PEER-REVIEWED | Posted: 30 March 2021 doi:10.20944/preprints202103.0720.v1

platforms for bioanalyte sensing have been applied in two distinct ways: (i) in-situ analyte monitoring whereby MN platform is used to interface ISF with on-device sensor component and (ii) extraction of dermal ISF using MNs coupled with various downstream analytical measurements, and [150].

5.1 In situ strategies

5.1.1 Electrochemical-based Microneedles

MNs integrated with electrochemical sensors are by far the most commonly reported MNs (MN)-based biosensing platforms, primarily due to the inherent advantages of electrochemical biosensors. Electrochemical sensing offers the most straightforward and robust approach from the standpoint of wearable and continuous on-device analyte monitoring devices. A major thrust in the development of MN-based electrochemical sensors came from the need to develop minimally invasive, pain-free continuous glucose monitoring (CGM) devices. Diabetes is a worldwide health problem and a significant cause of mortality and morbidity. Management of the disease's severe complications is largely possible if blood glucose levels are monitored regularly. However, currently available glucose monitoring methods are generally painful and not suited for repeat sampling and continuous on-body monitoring, hence the need for MN-based glucose level monitoring in dermal ISF.

Generally, electrochemical glucose sensing strategies can be divided into two categories: enzymatic and non-enzymatic. Glucose oxidase (GOx) is the most commonly used enzyme in enzymatic glucose sensors. Eq. 8 summarises the overall reaction where in the presence of oxidase (GOx), substrate (glucose) is oxidised to product (gluconic acid) and hydrogen peroxide (H_2O_2). Enzymatic biosensors for two other analytes, lactate and alcohol, also follow a similar reaction where respective oxidases: lactate oxidase (LOx) and alcohol oxidase (AOx) convert their respective substrates to corresponding products and H_2O_2.

$$Substrate + O_2 \xrightarrow{Oxidase} Product + H_2O_2 \quad (8)$$

Enzymatic glucose (also lactate and alcohol) sensors monitor either the consumption of O_2 in the reaction, or the amount of H_2O_2 produced due to glucose oxidation, thus providing an indirect measurement of glucose (analyte). Earlier reports on the use of MNs-based platforms for glucose sensing focused more on using MNs only to extract biofluid. For example, Mukerjee *et al*. developed an array of hollow single crystal silicon MNs, which are connected via microchannels to a reservoir on the opposite side of needle tips. A commercially available glucose testing strip coated with tetramethylbenzidine (TMB), GOx and horseradish peroxidase (HRP) was placed in contact with the extracted biofluid in the reservoir. H_2O_2 produced in the GOx mediated glucose oxidation reaction further reacts with the HRP and TMB on the strip, and colourimetric signal (change in colour of test strip from clear to deep blue) is generated by the well-known HRP catalysed TMB/ H_2O_2 redox reaction [63]. The authors tested their device on both whole blood and ISF.

Several MN-based glucose-sensing platforms have been reported that follow a general design: an array of hollow MNs that sample interstitial fluids from the epidermis, which is then transported to the enzymatic glucose biosensor integrated on the back side of the "needle-chip". Prominent examples of such a design include one of the earliest MN-based glucose-sensing platforms, reported by Zimmermann *et al*. Using 200 μm long hollow out-of-plane MNs, the ISF is pumped past a flow-through sensor chamber. Inside the sensor chamber, GOx is immobilised to the chamber surface upstream of the working electrode (WE) and catalyses the conversion of glucose to H2O2. The H_2O_2 is subsequently detected amperometrically using a typical 3-electrode system (Pt WE & CE, Ag/AgCl RE) [151]. Similarly, the method reported by Chua *et al*. tested the performance of two different MN designs using an integrated sensor chamber containing GOx coated Pt electrode as WE and Ag/AgCl as reference and counter electrodes [87]. With a slight modification in the way GOx is coated on the Pt electrode, the same sensor design was subsequently used

Preprints (www.preprints.org) | NOT PEER-REVIEWED | Posted: 30 March 2021 doi:10.20944/preprints202103.0720.v1

in a preliminary clinical study where 10 diabetic subjects wore the device for up to 72 hours, and the results were compared with fingerstick blood glucose readings [118]. A platform similar in design to the aforementioned ones, but for determination of K+ ions was reported. ISF was collected and transported to the integrated μfluidic chip by Eshell 300 hollow MNs. The solid-state ion-selective electrodes (ISEs) made up of 3D porous carbon were integrated into the μfluidic chip and used to determine K+ ion concentrations [124].

The platforms discussed so far are based on the so-called "first-generation glucose sensor" principle, where oxygen is used as a physiological electron acceptor. The active site of the GOx enzyme is its flavin adenine dinucleotide (FAD) redox centre embedded deep inside a thick protein layer. Thus, electrons' direct transfer between the GOx active site and electrode surface is not easily possible. Oxygen as an electron acceptor is a suitable choice for shuttling electrons between GOx redox centre and electrode surface due to its abundance in physiological conditions. However, as simple as this approach may appear, it is prone to errors primarily because of stoichiometric limitations of oxygen and oxygen tension fluctuations [152]. Insufficient oxygen for the glucose reaction will lead to inaccurate estimation of glucose levels. Several approaches have been devised to get around this oxygen dependence. One such approach which forms the basis of "second-generation glucose sensors" involves the use of non-physiological electron acceptors (mediators) instead of oxygen (Figure 5). Several electron mediators have been used in second-generation glucose sensors, such as ferricyanide. Strambini *et al*. coupled this sensing principle with their high-density silicon-dioxide hollow MN array. The sensor compartment integrated at the back of the needle-chip included screen-printed electrodes, with the working electrode modified with a layer comprised of GOx, hydrophilic polymer carboxymethylcellulose (CMC) and ferricyanide as electron acceptor.

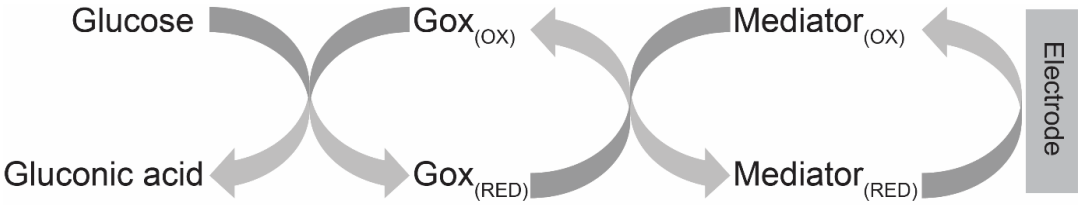

Figure 5. Principle of mediator based enzymatic glucose biosensors

Fabrication of such devices where a sensor is integrated with the patch/chip of hollow MNs as a separate compartment/pod is relatively complicated. Moreover, integration with flow microchannels for transport of fluid from the point of uptake to the sensor compartment is also a major impediment in using this design to develop wearable devices for on-body CGM [116]. Thus, more recent efforts have been focused on MNs based devices where sensing can be performed directly at the ISF-MN interface. Solid MNs coated with suitable electrode materials (discussed below) may offer an easy solution; however, lack of plasticity or amenability to further modifications with enzymes and mediators is a key challenge in this approach. In other cases, the lumen of hollow MNs is packed with suitable electrode materials and the electrode transducer is directly employed at the ISF-MN interface. For enzymatic biosensors, carbon paste electrodes have emerged as one of the most suitable options mainly due to their plasticity. Moreover, co-immobilisation of various sensor components like enzymes and mediators with the electrodes can be easily achieved. Consequently, several carbon paste-packed MN array devices have been reported for sensing of glucose and other analytes in ISF.

Miller *et al*. reported an MN array that could characterise the metabolic acidosis by multiplexed measurement of glucose, lactate, and pH in ISF. Individually addressable MNs within the array were modified to detect a single target. Rhodium modified carbon paste was used as a working electrode in combination with the respective enzymes (GOx or LOx) for glucose and lactate detection. On the other hand, the electrode for pH measurement was prepared by chemically depositing diazonium salt of Fast Blue RR on carbon

Preprints (www.preprints.org) | NOT PEER-REVIEWED | Posted: 30 March 2021 doi:10.20944/preprints202103.0720.v1

paste electrodes [153]. Valdés-Ramírez *et al*. reported a self-powered MN-based glucose sensor that utilised a carbon paste-based sensing (bioanode) electrode with co-immobilised GOx and mediator tetrathiafulvalene (TTF) [154]. Another unique feature of this device was that it utilised a Pt black cathode for catalysis of oxygen and harvesting sustainable power signals, Figure 6 [154]. A similar sensor was earlier reported by Windmiller *et al*. for lactate and H_2O_2. Rhodium dispersed (metallised) carbon paste was loaded into pyramidal MNs. Carbon paste also included LOx enzyme and polyethyleneimine (PEI) as stabiliser [116]. Carbon paste filled hollow MN array was also used in a proof-of-concept study for melanoma detection. Tyrosinase enzyme is a well-known melanoma biomarker that can be detected in ISF, and catechol is one of its substrates. Using hollow MNs filled with catechol coated carbon paste, the authors reported proof-of-concept *in vitro* evaluation of tyrosinase. Tyrosinase oxidises the catechol to Benzoquinone which can be detected by chronoamperometry (at a fixed potential of -250 mV vs Ag/AgCl) [126]. Another carbon paste filled hollow MN array was reported for continuous monitoring of Parkinson's disease drug Levodopa. This wearable MN device incorporated two independent, yet simultaneous sensing modalities within the same MN array. The MN array contained two WEs (CP), one of which was used for square wave voltammetry (SWV) based nonenzymatic detection of Levodopa, while the second WE was used for chronoamperometric detection of dopaquinone that is obtained as a product in enzymatic reaction of Levodopa with tyrosinase [155].

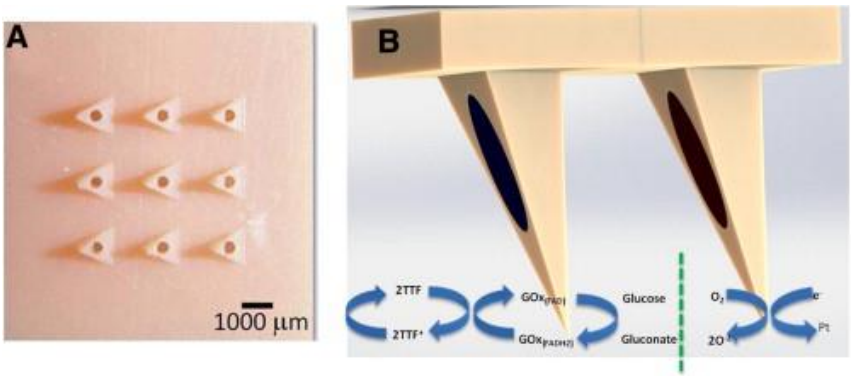

Figure 6. (A) optical micrograph of MN array. (B) Hollow MNs packed with carbon paste. Bioanode (left) was covered with CNT/TTF/GOx-BSA/glutaraldehyde/Nafion® layer. Cathode (right) was prepared by electrodepositing Pt–Rh alloy on bundles of carbon fibers followed by Nafion® dip coating. A schematic representation of reactions happening at each electrode is also shown. Reproduced with permission from Ref. [154].

More recently, Teymourian *et al*. have reported a carbon paste filled hollow MN array for multiplexed detection of glucose, lactate, and ketone bodies in ISF [156]. The array comprised of 4 MNs, with two being used as WEs, while the other two as RE and CE. β-hydroxybutyrate is a common marker for diabetic ketoacidosis diagnosis. In this paper, β-hydroxybutyrate (HB) detection was realised by NAD hydrogenase mediated oxidation of HB to acetylacetate, with concomitant reduction of NAD+ to NADH. NADH is subsequently detected amperometrically and gives an indirect measure of HB in the sample. From the sensing point of view, the authors incorporated several features in the MN sensor. Firstly, the WE to be used for HB detection used an ionic liquid-based carbon paste electrode with the mediator phenanthroline dione (PD) incorporate within the carbon paste. PD acts as an electron shuttling reagent for the regeneration of NAD+ from NADH. The ionic-liquid/CP/PD layer is coated with a mix of HBD and NAD+ crosslinked with the glutaraldehyde (GA). The ionic liquid provides stable confinement of NAD+ via hydrogen bonding and coulombic interaction between ionic liquid and NAD+. Furthermore, the ionic liquid also inhibits fouling of the electrode surface by the NADH produced as the product in HB detection reaction, Figure 7. Using PD as a mediator enables low potential NADH electrocatalysis and inhibition of leaching hydrogenase enzyme. Glucose/lactate

Preprints (www.preprints.org) | NOT PEER-REVIEWED | Posted: 30 March 2021 doi:10.20944/preprints202103.0720.v1

detection relied on GOx based oxidation of glucose to gluconic acid or LOx based conversion of lactate to pyruvate, along with the production of H_2O_2 in both reactions detected on the Prussian blue modified CP electrodes [156].

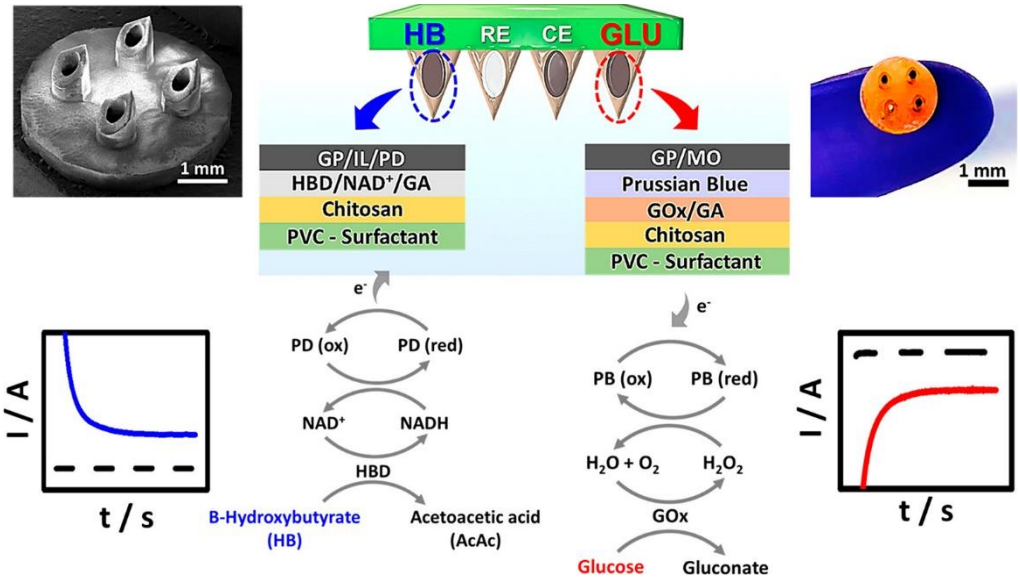

Figure 7. Top left: SEM image of the 2 × 2 arrays of hollow MNs. Top right: Optical image of the MN sensor. Middle: Schematic representation of multilayer modified dual- HB/GL sensor and the sensing mechanism. WE for HB (left) packed with GP/IL/PD and covered with HBD/NAD+/GA sensing layer. WE for GL (right) filled with GP/MO paste and covered with GOx/GA sensing layer. Another GP/MO packed MN was used as the CE, and a 500 µm Ag/AgCl wire-integrated MN used as the RE. Reproduced with permission from Ref. [156].

HB: β-Hydroxybutyrate, GL: Glucose, WE: Working electrode, IL: Ionic liquid, PD: Phenanthroline dione, HBD: β-Hydroxybutyrate dehydrogenase, GA: Glutaraldehyde, GP: Graphite powder, MO: Mineral oil, AcAc: Acetoactetic acid, GOx: Glucose oxidase.

Mohan *et al*. adopted a relatively different approach for employing an electrode transducer directly in contact with the hollow MN-ISF interface [125]. Instead of packing the lumen of hollow MN with carbon paste or any other material to be used as an electrode, solid Pt and Ag wires were integrated with pyramid-shaped hollow MNs. Pt wire, which is used as a sensing/working electrode, was modified layer by layer. First, o-phenylene diamine was electropolymerized on Pt wire followed by a layer of chitosan-AOx. Finally, an outer Nafion layer was created. The Nafion layer provides protection from leaching of biosensor components as well as acts as a barrier for negatively charged interferents, Figure 8 [125].

Preprints (www.preprints.org) | NOT PEER-REVIEWED | Posted: 30 March 2021 doi:10.20944/preprints202103.0720.v1

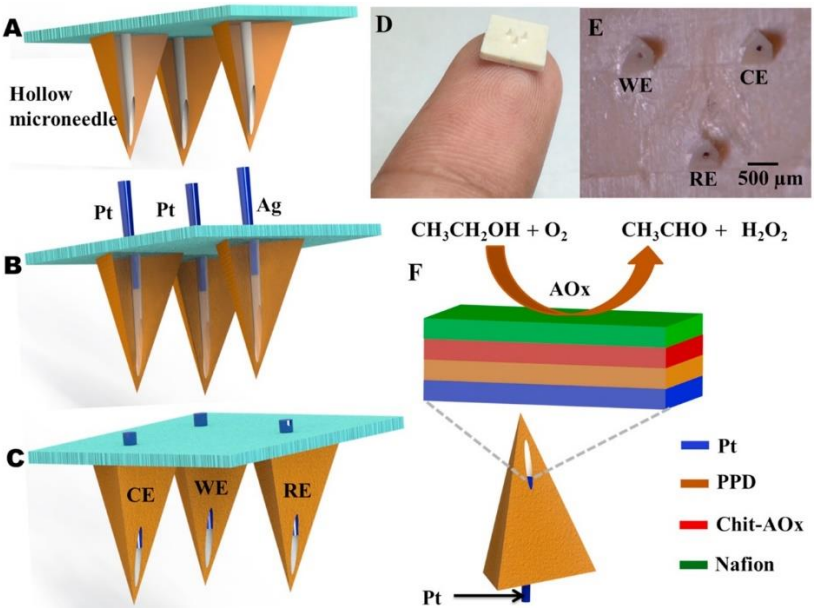

Figure 8. (A, B, C) MN array with integrated Pt (WE, CE) and Ag (RE) wires press fitted in to the aperture of hollow MN. (D) MN array mounted on the fingertip. (E) Optical micrograph of the MN array (F) Schematic representation of multi-layer alcohol biosensor and alcohol sensing mechanism. Reproduced with permission from Ref. [125].

Solid MNs are relatively easier to fabricate and are stronger and sharper as compared to hollow MNs. Thus, solid MNs hold immense potential to be used for inline detection of analytes. Another advantage of solid MNs is that based on the type of electrode/MN material used, they can be employed for both enzymatic and non-enzymatic analyte detection. For example, Barrett *et al*. reported an MN array made up of ultra-sharp gold-coated NOA68 polymer MNs. A 100 nm thick layer of gold was deposited thermally on the tip of MNs to enable direct electrochemical analysis at the MN tip. However, this MN platform did not immobilize/trap enzyme or mediator on the electrode surface. Instead, GOx and ferrocene monocarboxylic acid (FcCOOH) as an oxidising mediator were mixed with known concentrations of glucose and the amperometric signal was recorded using gold-coated MNs as WE and Pt wire and Ag/AgCl as counter and reference electrodes, respectively [157].

Another solid MN platform reported by Chen *et al*. employed stainless steel MNs. The MNs were then coated layer by layer with gold and platinum nanoparticles to enhance conductivity between the enzyme layer and the electrode. As oxygen concentration is about an order of magnitude less than glucose concentrations under physiological conditions, a few of the "second generation glucose sensors" employ transport limiting membranes/layers to limit glucose concentration reaching the electrode surface. In this report by Chen *et al*., electrodes were also covered by two layers of biocompatible coating: porous PVDF layer, and nanosphere Nafion layer, to limit the concentration of glucose reaching electrode, thus circumventing the oxygen deficiency issue. GOx enzyme was electrostatically trapped in Polyaniline film, which was placed between the PVDF layer and the Pt nanoparticle layer [158]. Caliò and co-workers reported another solid MN-based multi-analyte (glucose and lactate) sensing platform where working electrodes were fabricated by standard photolithography of a mixture of poly(ethylene glycol) diacrylate (PEGDA), enzyme (GOx or LOx), electron mediator vinylferrocene (VF), and photoinitiator Darocur© [159]. A similar multianalyte biosensor for monitoring glucose and lactate in ISF was reported by Bollella and co-workers where the surface of MNs was electrodeposited with Au-multiwalled carbon nanotubes (MWCNTs). Electron mediator methylene blue (MB) was electropolymerized to poly-methylene blue (pMB). Au-MWCNTs/pMB electrodes were individually functionalized by drop-casting the relevant enzyme (LOx, or FAD-glucose dehydrogenase). Yet another enzymatic glucose sensor platform based on functionalized solid MNs was reported by Sharma *et al*. Metallised epoxy-based negative

 doi:10.20944/preprints202103.0720.v1

photoresist (SU-8 50) was used to fabricate MN array. For working electrode, the SU-8 50 was metallised with Pt while for reference electrode SU-8 50 was metallised by silver. GOx was trapped in electropolymerized polyphenol (PP) film [160].

Non-enzymatic glucose-sensing offers several advantages compared to the use of enzymatic sensors. Non-enzymatic sensors are relatively stable and easy to fabricate and are not affected by oxygen limitation. Non-enzymatic glucose-sensing appears to be particularly suited for solid MN-based platforms. Platinum black as electrode material for non-enzymatic glucose sensing has attracted much interest because of its biocompatibility and high catalytic activity. At least two solid MN platforms for non-enzymatic sensing of glucose in ISF have been reported in recent years. Lee *et al*. developed a patch shaped 3D SUS MN electrode array. MNs were made by micromachining of commercial stainless steel 316L grade substrate. Pt black and Ag/AgCl were electroplated on the tip of each MN (as working and counter/reference electrodes, respectively), and glucose concentration was measured chronoamperometrically at a fixed potential of 400 mV vs Ag/AgCl [85]. Similarly, Chinnadayyala and co-workers reported a stainless MN array where the tips of MNs were gold coated. The working electrode was sequentially coated with Nafion and Pt black. Nafion membrane provides a selective barrier for many of the non-specific interferents. In addition to the use of Nafion for improved specificity of detection, this platform also featured low potential (120 mV) non-enzymatic glucose detection with a response time of just 2 seconds. The sensor showed high selectivity for glucose even in the presence of 10-fold excess of common interferents ascorbic acid, lactic acid, dopamine, uric acid, and acetaminophen [111].

The application of solid MN arrays for enzyme-free detection of biomolecules/metabolites is not limited to glucose only. Skoog *et al*. reported an MN platform for enzyme-free determination of two important metabolites, uric acid and dopamine. Increased uric acid levels are associated with a range of diseases like diabetes, arthritis, gout, and cardiovascular diseases etc. Dopamine, on the other hand, has been used to investigate Parkinson's disease and schizophrenia. The authors coated titanium alloy MNs with nitrogen-doped ultrananocrystalline diamond (N-UNCD). The choice of doped diamond electrodes was dictated by their several superior electrochemical properties like low background, wide potential, high current density electrolysis, low detection limits, and response stability etc. The transdermal biosensing application of MN array was demonstrated *in vitro* through porcine skin penetration testing and linear sweep voltammetric detection (potential window −0.2 V to 0.8 V at a scan rate of 10 mV/s) of uric acid and dopamine [161].

Due to the versatility and ease of fabrication, solid MN arrays have been used in sensors for a range of other biomolecules, for example, the concentration of β-lactam antibiotics in human ISF. This β-lactam sensor consists of gold (working electrode) and silver (reference electrode) coated poly(carbonate) MN arrays. A pH-sensitive layer was subsequently created on working electrodes by electrodepositing iridium oxide. An enzyme hydrogel made up of β-lactamase, poly(ethylenimine) (PEI), glycerol, and poly(ethylene glycol) diglycidyl ether (PEG-DE) dissolved in 10 mM PBS was applied on top of iridium oxide layer. The sensor's working principle was based on using iridium oxide to detect changes in local pH, which may result from the hydrolysis of β-lactam by β-lactamase [83,103].

McConville and Davis demonstrated a proof-of-concept solid MN array made up by encapsulating microparticulate (<1 μm diameter) Palladium composite with a polymer binder (polycarbonate or polystyrene). The transdermal sensing application was demonstrated using a calcium alginate hydrogel skin mimic loaded with redox probe ferrocyanide [162]. Another proof-of-concept MN array was reported where the authors adopted a unique approach for reagent-less determination of pH in ISF. The approach involved using electrochemical anodisation of carbon loaded polystyrene MNs to increase the population of endogenous quinone functionalities at the interface of carbon.

Quinone groups show pH-dependent redox transitions, which can be exploited for reagent -less determination of pH [163]. The concept of electrochemical sensors based on

Preprints (www.preprints.org) | NOT PEER-REVIEWED | Posted: 30 March 2021 doi:10.20944/preprints202103.0720.v1

micro-interfacial interaction between the sensor and the analyte was also explored in another MN array sensor. Although the MN array used to develop this sensor comprised of hollow MNs in contrast to the aforementioned pH sensor, the sensing mechanism between the two methods is similar in the sense that the electrode surface was electrochemically "sensitized" to respond to the analyte present in the sample fluid. When a potential difference is applied to organogel filled hollow MNs immersed in sample fluid, ion transfer occurs across the polarised organogel/fluid interface. The resultant current can be monitored and mirrors the analyte concentration. The application of this MN array was demonstrated for detection of propranolol in physiological medium by differential pulse voltammetry [164].

5.1.2 Surface-Enhanced Raman Spectroscopy (SERS)

Surface-enhanced Raman Spectroscopy (SERS) is highly sensitive molecular detection technique. However, its integration with MN arrays has been limited primarily because of the possible biofouling of plasmonically enhancing substrates. Park *et al*. demonstrated that integrating plasmonically enhanced gold nanorods with polymeric MN array can effectively monitor pH in artificial ISF. Coating plasmonic MNs with pH-sensitive 4-mercaptobenzoic acid (4-MBA) can enable monitoring of pH in a variety of samples. 4-MBA is protonated at acidic pH (pH 2) while it is deprotonated at basic pH (pH 12) [95]. The invention of flexible plasmonic substrates, also called "plasmonic paper" paved the way for the integration of SERS based detection with MN array and wearable devices. Plasmonic paper is made by immobilizing plasmonic nanostructures on filter paper. Recently, Kolluru *et al*. reported an MN patch integrated with plasmonic paper. Polystyrenesulfonate (PSS) coated gold nanorods were immobilized on a thin strip of filter paper via plasmonic calligraphy. Using Rhodamine 6G (R6G) as a model compound, the proof-of-concept application of this MN patch was demonstrated for patch molecule detection in dermal ISF. PSS is negatively charged, which can bind and localize positively charged (R6G), which can be further detected by acquiring SERS spectra. Although this approach's utility was demonstrated by monitoring the pharmacokinetics profile of R6G in serum and dermal ISF, extensive work may be needed to develop flexible plasmonic substrates that can detect other more common biomolecules with high specificity [165].

5.2 Ex-situ strategies

Ex-situ monitoring of biomolecular components of various biofluids is currently the most commonly adopted approach. Despite the apparent fact that ex-situ biomolecule monitoring using MNs may not be of high utility in clinical practice, from the standpoint of discovery research, minimally invasive and pain-free extraction of sufficient quantities of ISF can prove to be highly beneficial. Conventional ISF collection methods like suction blisters or implantation of tubing not only put the patients under unnecessary stress, they are time-consuming and sometimes require local anaesthesia and experienced workers [41]. In contrast, MN-based sampling of ISF offers a simpler and minimally invasive approach and can thus immensely expand the scope of ISF based basic research. A few of the earlier biomolecular sensing approaches used MN-based ISF sampling only while the detection and quantification of biomolecule were carried out ex-situ. For example, Wang *et al*. reported a glass MN array for the sampling of dermal ISF. After the insertion of the MN array to micrometre depths in the skin, the ISF was extracted by applying a vacuum of 200-500 mm Hg for 5-10 minutes. Glucose concentrations in extracted ISF were measured by a commercial glucose test strip [62].

The application of MN arrays for profiling of biomolecular content of the ISF has recently been reported in two comprehensive reports. Tran *et al*. used arrays of commercially available 32G ultrafine nano pen needles and collected ISF from healthy human subjects. The proteomic content of extracted ISF was subsequently analysed by liquid chromatography mass spectrometry (LC-MS/MS) analysis. The authors identified a total of over 3000 proteins in the ISF. When compared with the proteomic profile of the subjects' serum, less than 1% of which were found to be unique for ISF [166]. Similarly, Miller *et al*.

Preprints (www.preprints.org) | NOT PEER-REVIEWED | Posted: 30 March 2021 doi:10.20944/preprints202103.0720.v1

used the in-house constructed array of commercially available nano pen needles and extracted ISF from human subjects and rats. This is one of the most comprehensive reports on biomolecular profiling of MN-extracted ISF. The authors analysed proteomic and transcriptomic profiles in ISF and compared them with plasma and serum collected from the same subjects. Remarkably, the authors, for the first-time, reported isolation and characterization of exosomes from ISF [144].

6. Integrated microfluidic-based MN arrays for sampling and sensing ISF

An MN array patch integrated into the microfluidic system offers a better solution for wearable sensing. The approach provides non-invasive investigation when coupled with a suitable driving force to collect the skins' fluid. MNs array integrated with the microfluidic system needs to address reliable and repeatable measurements of ISF. The integrated system needs to analyse the flow at low volume, avoid dilution, and maintain minimum contamination [167,168]. Microfluidic chip may incorporate electrochemical sensing by guiding the fluids into the micro-channel with integrating MNs array. However, various factors may affect the performance of the MNs array. They include the type of material, height, tip-radius, diameter, needle shape, and density [169]. Besides, mechanical and biological optimisation is crucial to validate the constructed MNs on the human skin.

Takeuchi *et al*. demonstrated the extraction of ISF through porous MNs made of hyaluronic acid (HA) coated PDMS. The array consisted 21 MNs with a length of 1000 μm each [61]. The MNs array penetrated the agarose gel phantom and extracted the ISF for further investigations. A continuous flow of ISF was established in the device by capillary action utilising manual compression. A minimum flowrate of >(1-2) μL/min was needed to detect the changes in glucose concentration. Samant *et al*. collected >1 μL of ISF within 20 min from pig cadaver skin and living human subjects utilising MNs patches [41]. The patches contained an array of solid, porous, and hollow MNs that penetrated the superficial skin layers. They suggested that diffusion offered better extraction when hydrogel-based porous MNs were used. The capillary driving force or osmosis force offered better extraction when hollow MNs were used.

Miller *et al*. reported an array of hollow MNs that extracted 20 μL and 60 μL of dermal ISF from human and rat subjects, respectively [60]. The 5 MNs array had a length of 1500 μm each. Up to 16 μL of ISF was extracted in 2h from human subjects. However, a replacement of MNs was necessary to extract a higher volume of ISF (>30-60 μL). Liu *et al*. demonstrated a device incorporating a microfluidic base, an integrated sensor for glucose detection, and a pressure module to sample the ISF [57]. The system extracted ample ISF using an ultrafiltration (UF) probe *in vivo*. The extracted ISF was analysed to detect glucose concentration. Negative pressure was used to extract and discharge the ISF after each measurement.

Ribet *et al*. reported a single stainless MN-based sampling device that could extract 1 μL of ISF from the human forearm [170]. The MNs were connected to a microfluidic chip incorporating a paper matrix. The extracted biofluid was stored in the paper matrix. The analysis was done off-chip with mass spectrometry (LC-MS/MS). Lee *et al*. devised a porous MNs array made of PDMS, Figure 9A. Mould casting and salt leaching methods were used to fabricate the MNs [130]. The MNs array was integrated into a paper-based enzymatic colourimetric glucose sensor via a microfluidic channel. The array consisted 21 MNs with a length of 800 μm. The colour of the filter paper changed according to the concentration of glucose. The fluid was extracted from the agarose gel.

Mukerjee *et al*. demonstrated a hollow MNs array with a height of 250-350 μm [63]. The array was connected to a microchannel system, Figure 9B. The microchannel had a common reservoir to collect the ISF. The MNs successfully penetrated the living epithelial layer to access the ISF. The flow was induced by capillary action. The glucose concentration of the ISF was validated by in-situ measurements.

Trzebinski *et al*. reported a solid MNs array (named micro-spikes) to sense the clinically relevant substrate such as glucose and lactose in the ISF, Figure 9C [166]. The array

Preprints (www.preprints.org) | NOT PEER-REVIEWED | Posted: 30 March 2021 doi:10.20944/preprints202103.0720.v1

was coated with an enzyme layer for biosensing. The enzyme layer was made of glucose oxidase or lactose oxidase on top of the gold layer. This offered an improved sensitivity due to the higher signal to noise ratio. The microspike platform was integrated with the microfluidic chip to observe the transported biomolecule.

Kolluru *et al*. presented an array consisting of 9 MNs to extract the ISF from the rat dermis [112]. The array was attached to a thin strip of filter paper that absorbed the ISF for subsequent investigations. The fabricated MNs with a length of 650 μm were able to collect >2 μL of ISF within 1 min. However, the MNs array was repeatedly applied to the skin to augment the extraction of ISF, which may not be suitable for the application in human subjects. Later the group improved the system by incorporating a plasmonic paper as shown in Figure 9D [165]. The paper was immobilised with poly-styrenesulfonate (PSS) coated gold nanorods (AuNRs). The absorbed ISF in the paper was investigated by Surface-Enhanced Raman scattering (SERS). Pharmacokinetic profiles of Rhodamine 6G (R6G) from the ISF was detected and quantified from the rat's dermis.

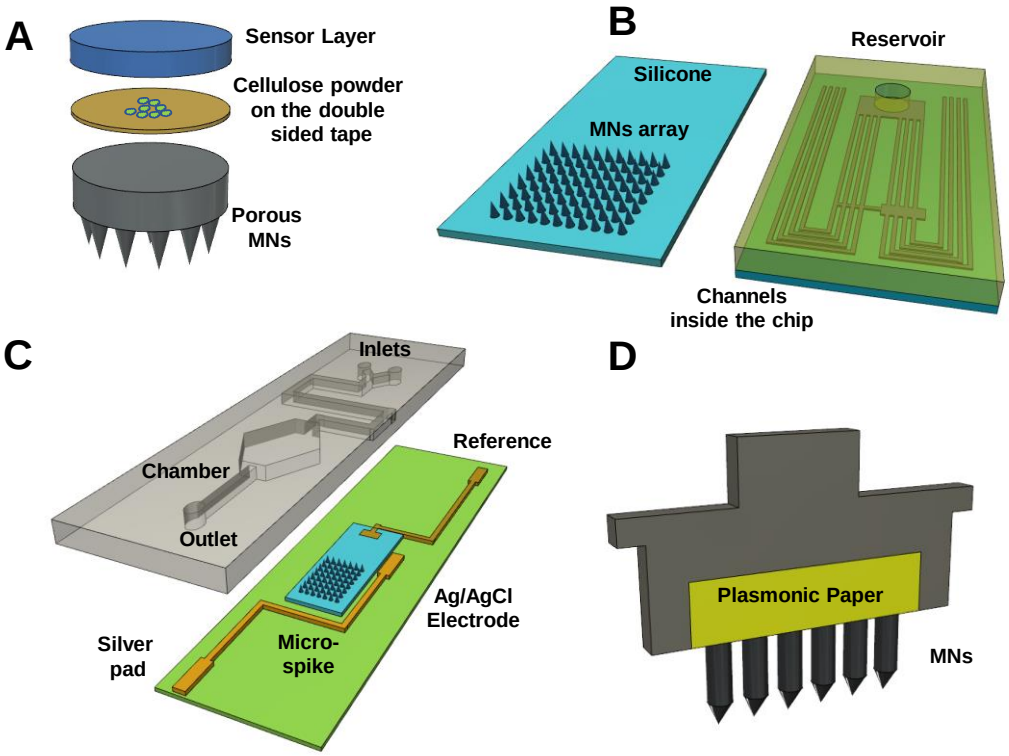

Figure 9. Integrated MNs arrays with the microfluidic system (A) A porous MNs array made of PDMS. The array is connected to a paper-based colourimetric glucose sensors [130], (B) A hollow MNs array connected to a set of microchannels, and a common reservoir [63], (C) Solid MNs array (micro-spike) coated with enzyme layer [166]. The MNs array was connected to a microfluid system for further investigations, and (D) MNs array attached to a plasmonic paper [165]. The absorbed ISF in the paper was investigated by Surface-Enhanced Raman Scattering (SERS). Figures were redrawn from Refs. [130], [63], [166] and [165], respectively. Figures are not drawn to scale.

7. Challenges and possible solutions of ISF sampling from skin

Collecting an ample amount of ISF is challenging due to the complex nature of the human body's transport system. Most of the skin's ISF is found in the dermal region [171]. Comparing to the blood (order of 5L), ISF is in order of 17L on average for an adult human [5]. Yet, collecting an ample amount of ISF to detect specific biomarkers is challenging. This is due to the small pockets of tiny drops (micrometre-sized layer) lying between the interstitial space. Furthermore, ISF is retained in the tissue, and pricking by MNs does not spontaneously extract the fluids. This results in a slower extraction of ISF compared to the blood. Comparing to the blood glucose, detecting glucose in ISF involves a measurement

Preprints (www.preprints.org) | NOT PEER-REVIEWED | Posted: 30 March 2021 doi:10.20944/preprints202103.0720.v1

delay of 20-35 min. This is due to the slow transport rate of glucose in ISF. For instance, it requires almost 20-35 minutes for the glucose molecules to travel only 1 mm in the ISF. Thus, an improved sensing platform needs to be developed to reduce measurement delays. Moreover, wearable microneedles coated with related analytes for in-situ ISF analysis can address most of these issues.

A report from the Human Society International suggests that less than 10% of the conducted research from animal studies is effective and safe in clinical trials in humans [172]. Therefore, it is very crucial to develop a universal *in vitro* skin model to mimic the *in vivo* ISF flow. This can bridge the gap between animal studies and human trials. A universal skin model can significantly improve the viabilities of different extraction techniques of the ISF [173]. Challenges rely on replicating the *in vivo* environments and their response to external stimuli, stretching, and shear stresses [174]. Moreover, developing a portable and integrated dynamic flow system is essential with the current skin model for the realistic supply and drainage of ISF [175]. Gravity induced flow may provide a portable and cost-effective solution. However, they may not offer a dynamic flow behaviour in the complex model. Therefore, it is essential to improve the biofluids' current transport system by avoiding the bulky fluids setup.

8. Conclusion and Perspectives

Using ISF instead of other biofluids such as blood, urine, sweat and saliva for detection and disease monitoring has emerged rapidly. However, ISF has several inherent challenges. For example, unlike blood, the ISF extraction is time-consuming and may take up to hours. Also, the amount of dermal ISF that can be collected is low, making it difficult for standard lab-based analysis. On the other hand, the synergistic combination of ISF detection and microfluidic technology can address most of these challenges, leading to enormous progress in this field.

Herein, we systematically discussed the cutting-edge advances in various aspects of MNs for ISF collection and sensing. We first discuss the ISF collection mechanism and briefly investigated the pros and cons of conventional ISF collection methods compared to MN ISF sampling approach. Then, essential design considerations for MNs were overviewed, and special attention was paid to mechanical design and biocompatibility analysis of MNs. Next, the fabrication technologies of the four most common MNs for ISF collection were thoroughly explained. We also identified the challenges associated with these fabrication techniques. Next, we elaborated on sampling methods for ISF collection as well as various sensing mechanisms for ISF detection. Most importantly, the integrated microfluidic-based MN arrays for sampling and sensing ISF were presented. Finally, we identified the possible challenges in dermal ISF extraction and offered possible solutions.

Microfluidic technology can offer significant improvements in ISF sampling and detection in three main areas: (i) Painless MNs for collecting decent amounts of ISF in a short duration; (ii) Improving the *in situ* and continuous ISF collection and detection by offering wearable MNs integrated with biosensors. (iii) Providing a more realistic *in vitro* skin model for ISF flow.

At present, there is a lack of MNs array-based integrated microfluidic systems mimicking an *in vitro* skin model for ISF flow. More research needs to be initiated to develop an integrated system for on-chip ISF sampling and analysis. The design consideration needs to be such that minimum contamination and infection risks are associated. This will reduce the live animal and human trials and provide more thorough studies for toxicity, metabolism, and putative drug tests before entering the clinical trials [176]. The integrated system needs to offer both the on-skin and off-skin investigation to reduce human trials.

The future of the point-of-care diagnostic device needs to be non-invasive. Tissue injuries need to be minimised while maintaining the patient's comfort with reliable data. The following key considerations need to be addressed: (i) painless access to ISF, (ii) reduced sampling time and delay, (iii) simplicity and low cost, (iv) reduced contamination, (v) enough analyte for subsequent measurement and quantification, and (vi) accurate measurements. A microfluidic chip with a multi-layer platform could mimic the full-

 doi:10.20944/preprints202103.0720.v1

thickness skin model [177]. Each of the layers may incorporate a standalone microchannel to perfuse the blood, plasma, or ISF flow. It will be interesting to investigate the perfusion of different biofluid within the same system and their effect on the skin model

Author Contributions: N.K. and N.-T.N. developed the structure of the paper. Other authors collected and analysed the literature. All authors wrote the paper.

Funding: This research received no external funding

Institutional Review Board Statement: Not applicable.

Informed Consent Statement: Not applicable.

Conflicts of Interest: The authors declare no conflict of interest.

References

1. Yao, W.; Li, Y.; Ding, G. Interstitial fluid flow: the mechanical environment of cells and foundation of meridians. *Evidence-Based Complementary and Alternative Medicine* **2012**, *2012*.
2. Aukland, K.; Nicolaysen, G. Interstitial fluid volume: local regulatory mechanisms. *Physiological reviews* **1981**, *61*, 556-643.
3. Scallan, J.; Huxley, V.H.; Korthuis, R.J. Capillary fluid exchange: regulation, functions, and pathology. In Proceedings of the Colloquium Lectures on Integrated Systems Physiology-\nl\hspace* 18pt From Molecules to Function, 2010; pp. 1-94.
4. Sansalone, V.; Kaiser, J.; Naili, S.; Lemaire, T. Interstitial fluid flow within bone canaliculi and electro-chemo-mechanical features of the canalicular milieu. *Biomechanics and modeling in mechanobiology* **2013**, *12*, 533-553.
5. Corrie, S.R.; Coffey, J.; Islam, J.; Markey, K.; Kendall, M. Blood, sweat, and tears: developing clinically relevant protein biosensors for integrated body fluid analysis. *Analyst* **2015**, *140*, 4350-4364.
6. Ebah, L.M.; Wiig, H.; Dawidowska, I.; O'toole, C.; Summers, A.; Nikam, M.; Jayanti, A.; Coupes, B.; Brenchley, P.; Mitra, S. Subcutaneous interstitial pressure and volume characteristics in renal impairment associated with edema. *Kidney international* **2013**, *84*, 980-988.
7. Steil, G.; Rebrin, K.; Hariri, F.; Jinagonda, S.; Tadros, S.; Darwin, C.; Saad, M. Interstitial fluid glucose dynamics during insulin-induced hypoglycaemia. *Diabetologia* **2005**, *48*, 1833-1840.
8. Munson, J.M.; Shieh, A.C. Interstitial fluid flow in cancer: implications for disease progression and treatment. *Cancer management and research* **2014**, *6*, 317.
9. Munaz, A.; Shiddiky, M.J.; Nguyen, N.-T. Magnetophoretic separation of diamagnetic particles through parallel ferrofluid streams. *Sensors and Actuators B: Chemical* **2018**, *275*, 459-469.
10. Soltani, M.; Chen, P. Numerical modeling of interstitial fluid flow coupled with blood flow through a remodeled solid tumor microvascular network. *PloS one* **2013**, *8*, e67025.
11. Shieh, A.C.; Swartz, M.A. Regulation of tumor invasion by interstitial fluid flow. *Physical biology* **2011**, *8*, 015012.
12. Welter, M.; Rieger, H. Interstitial fluid flow and drug delivery in vascularized tumors: a computational model. *PloS one* **2013**, *8*, e70395.
13. Heldin, C.-H.; Rubin, K.; Pietras, K.; Östman, A. High interstitial fluid pressure—an obstacle in cancer therapy. *Nature Reviews Cancer* **2004**, *4*, 806-813.
14. Kim, J.; Campbell, A.S.; Wang, J. Wearable non-invasive epidermal glucose sensors: A review. *Talanta* **2018**, *177*, 163-170.
15. Kashaninejad, N.; Nguyen, N.-T.; Chan, W.K. Engineering Micropatterned Surfaces for Controlling the Evaporation Process of Sessile Droplets. *Technologies* **2020**, *8*, 29.
16. Kashaninejad, N.; Yaghoobi, M.; Pourhassan-Moghaddam, M.; Bazaz, S.R.; Jin, D.; Warkiani, M.E. Biological Diagnosis Based on Microfluidics and Nanotechnology. In *Nanotechnology and Microfluidics*; 2020; pp. 211-238.

17. Maleki, M.A.; Soltani, M.; Kashaninejad, N.; Nguyen, N.-T. Effects of magnetic nanoparticles on mixing in droplet-based microfluidics. *Physics of Fluids* **2019**, *31*, 032001, doi:10.1063/1.5086867.
18. Maleki, M.A.; Zhang, J.; Kashaninejad, N.; Soltani, M.; Nguyen, N.-T. Magnetofluidic spreading in circular chambers under a uniform magnetic field. *Microfluidics and Nanofluidics* **2020**, *24*, 80, doi:10.1007/s10404-020-02387-7.
19. Tajik, P.; Saidi, M.S.; Kashaninejad, N.; Nguyen, N.-T. Simple, Cost-Effective, and Continuous 3D Dielectrophoretic Microchip for Concentration and Separation of Bioparticles. *Industrial & Engineering Chemistry Research* **2020**, *59*, 3772-3783, doi:10.1021/acs.iecr.9b00771.
20. Yadav, S.; Kashaninejad, N.; Nguyen, N.-T. RhoA and Rac1 in Liver Cancer Cells: Induction of Overexpression Using Mechanical Stimulation. *Micromachines* **2020**, *11*, 729.
21. Moshksayan, K.; Kashaninejad, N.; Saidi, M.S. Inventions and Innovations in Preclinical Platforms for Cancer Research. *Inventions* **2018**, *3*, 43.
22. Taghibakhshi, A.; Barisam, M.; Saidi, M.S.; Kashaninejad, N.; Nguyen, N.-T. Three-Dimensional Modeling of Avascular Tumor Growth in Both Static and Dynamic Culture Platforms. *Micromachines* **2019**, *10*, 580.
23. Sheidaei, Z.; Akbarzadeh, P.; Kashaninejad, N. Advances in numerical approaches for microfluidic cell analysis platforms. *Journal of Science: Advanced Materials and Devices* **2020**, *5*, 295-307, doi:https://doi.org/10.1016/j.jsamd.2020.07.008.
24. Barisam, M.; Saidi, M.S.; Kashaninejad, N.; Vadivelu, R.; Nguyen, N.-T. Numerical Simulation of the Behavior of Toroidal and Spheroidal Multicellular Aggregates in Microfluidic Devices with Microwell and U-Shaped Barrier. *Micromachines* **2017**, *8*, 358.
25. Yaghoobi, M.; Saidi, M.S.; Ghadami, S.; Kashaninejad, N. An Interface–Particle Interaction Approach for Evaluation of the Co-Encapsulation Efficiency of Cells in a Flow-Focusing Droplet Generator. *Sensors* **2020**, *20*, doi:10.3390/s20133774.
26. Ebadi, M.; Moshksayan, K.; Kashaninejad, N.; Saidi, M.S.; Nguyen, N.-T. A tool for designing tree-like concentration gradient generators for lab-on-a-chip applications. *Chemical Engineering Science* **2020**, *212*, 115339, doi:https://doi.org/10.1016/j.ces.2019.115339.
27. Rismanian, M.; Saidi, M.S.; Kashaninejad, N. A microfluidic concentration gradient generator for simultaneous delivery of two reagents on a millimeter-sized sample. *Journal of Flow Chemistry* **2020**, *10*, 615-625, doi:10.1007/s41981-020-00104-7.
28. Mahmudunnabi, R.G.; Farhana, F.Z.; Kashaninejad, N.; Firoz, S.H.; Shim, Y.-B.; Shiddiky, M.J.A. Nanozyme-based electrochemical biosensors for disease biomarker detection. *Analyst* **2020**, *145*, 4398-4420, doi:10.1039/D0AN00558D.
29. Soda, N.; Umer, M.; Kashaninejad, N.; Kasetsirikul, S.; Kline, R.; Salomon, C.; Nguyen, N.-T.; Shiddiky, M.J.A. PCR-Free Detection of Long Non-Coding HOTAIR RNA in Ovarian Cancer Cell Lines and Plasma Samples. *Cancers* **2020**, *12*, 2233.
30. Henry, S.; McAllister, D.V.; Allen, M.G.; Prausnitz, M.R. Microfabricated Microneedles: A Novel Approach to Transdermal Drug Delivery. *Journal of Pharmaceutical Sciences* **1998**, *87*, 922-925, doi:https://doi.org/10.1021/js980042+.
31. Nguyen, N.-T.; Shaegh, S.A.M.; Kashaninejad, N.; Phan, D.-T. Design, fabrication and characterization of drug delivery systems based on lab-on-a-chip technology. *Advanced Drug Delivery Reviews* **2013**, *65*, 1403-1419, doi:https://doi.org/10.1016/j.addr.2013.05.008.
32. Xie, L.; Zeng, H.; Sun, J.; Qian, W. Engineering Microneedles for Therapy and Diagnosis: A Survey. *Micromachines* **2020**, *11*, 271.
33. Wang, Z.; Luan, J.; Seth, A.; Liu, L.; You, M.; Gupta, P.; Rathi, P.; Wang, Y.; Cao, S.; Jiang, Q.; et al. Microneedle patch for the ultrasensitive quantification of protein biomarkers in interstitial fluid. *Nature Biomedical Engineering* **2021**, *5*, 64-76, doi:10.1038/s41551-020-00672-y.
34. Teymourian, H.; Tehrani, F.; Mahato, K.; Wang, J. Lab under the Skin: Microneedle Based Wearable Devices. *Adv Healthc Mater n/a*, 2002255, doi:https://doi.org/10.1002/adhm.202002255.
35. Takeuchi, K.; Kim, B. Functionalized microneedles for continuous glucose monitoring. *Nano Convergence* **2018**, *5*, 28, doi:10.1186/s40580-018-0161-2.

36. Zhang, B.L.; Zhang, X.P.; Chen, B.Z.; Fei, W.M.; Cui, Y.; Guo, X.D. Microneedle-assisted technology for minimally invasive medical sensing. *Microchemical Journal* **2021**, *162*, 105830, doi:https://doi.org/10.1016/j.microc.2020.105830.
37. García-Guzmán, J.J.; Pérez-Ràfols, C.; Cuartero, M.; Crespo, G.A. Microneedle based electrochemical (Bio)Sensing: Towards decentralized and continuous health status monitoring. *TrAC - Trends in Analytical Chemistry* **2021**, *135*, doi:10.1016/j.trac.2020.116148.
38. Chary, S.R.; Jain, R.K. Direct measurement of interstitial convection and diffusion of albumin in normal and neoplastic tissues by fluorescence photobleaching. *Proceedings of the National Academy of Sciences* **1989**, *86*, 5385-5389.
39. Zhang, D.; Ding, G.; Shen, X.; Yao, W.; Zhang, Z.; Zhang, Y.; Lin, J.; Gu, Q. Role of mast cells in acupuncture effect: a pilot study. *Explore* **2008**, *4*, 170-177.
40. Tsay, R.-Y.; Weinbaum, S. Viscous flow in a channel with periodic cross-bridging fibres: exact solutions and Brinkman approximation. *Journal of Fluid Mechanics* **1991**, *226*, 125-148.
41. Samant, P.P.; Prausnitz, M.R. Mechanisms of sampling interstitial fluid from skin using a microneedle patch. *Proceedings of the National Academy of Sciences* **2018**, *115*, 4583-4588.
42. Hsu, H.-H.; Schimek, K.; Marx, U.; Pörtner, R. Measurement and simulation of permeation and diffusion in native and cultivated tissue constructs. *Biomaterials in Regenerative Medicine* **2018**, 245.
43. Knorr, F.; Lademann, J.; Patzelt, A.; Sterry, W.; Blume-Peytavi, U.; Vogt, A. Follicular transport route–research progress and future perspectives. *European Journal of Pharmaceutics and Biopharmaceutics* **2009**, *71*, 173-180.
44. Bandodkar, A.J.; Jeerapan, I.; Wang, J. Wearable chemical sensors: Present challenges and future prospects. *Acs Sensors* **2016**, *1*, 464-482.
45. Lee, H.; Choi, T.K.; Lee, Y.B.; Cho, H.R.; Ghaffari, R.; Wang, L.; Choi, H.J.; Chung, T.D.; Lu, N.; Hyeon, T. A graphene-based electrochemical device with thermoresponsive microneedles for diabetes monitoring and therapy. *Nature nanotechnology* **2016**, *11*, 566.
46. Lee, H.; Song, C.; Hong, Y.S.; Kim, M.S.; Cho, H.R.; Kang, T.; Shin, K.; Choi, S.H.; Hyeon, T.; Kim, D.-H. Wearable/disposable sweat-based glucose monitoring device with multistage transdermal drug delivery module. *Science Advances* **2017**, *3*, e1601314.
47. Kiistala, U. Suction blister device for separation of viable epidermis from dermis. *J Invest Dermatol* **1968**, *50*, 129-137.
48. Niedzwiecki, M.M.; Samant, P.; Walker, D.I.; Tran, V.; Jones, D.P.; Prausnitz, M.R.; Miller, G.W. Human suction blister fluid composition determined using high-resolution metabolomics. *Analytical chemistry* **2018**, *90*, 3786-3792.
49. Yu, H.; Li, D.; Roberts, R.C.; Xu, K.; Tien, N.C. An interstitial fluid transdermal extraction system for continuous glucose monitoring. *Journal of microelectromechanical systems* **2012**, *21*, 917-925.
50. Zhao, R.; Wang, C.; Lu, F.; Du, L.; Fang, Z.; Guo, X.; Liu, J.-T.; Chen, C.-J.; Zhao, Z. A Flexible Interdigital Electrode Used in Skin Penetration Promotion and Evaluation with Electroporation and Reverse Iontophoresis Synergistically. *Sensors* **2018**, *18*, 1431.
51. Kim, J.; Sempionatto, J.R.; Imani, S.; Hartel, M.C.; Barfidokht, A.; Tang, G.; Campbell, A.S.; Mercier, P.P.; Wang, J. Simultaneous monitoring of sweat and interstitial fluid using a single wearable biosensor platform. *Advanced Science* **2018**, *5*, 1800880.
52. Li, S.K.; Ghanem, A.H.; Peck, K.D.; Higuchi, W.I. Characterization of the transport pathways induced during low to moderate voltage iontophoresis in human epidermal membrane. *Journal of pharmaceutical sciences* **1998**, *87*, 40-48.
53. Chang, J.H.; Hogan, N.C.; Hunter, I.W. A needle-free technique for interstitial fluid sample acquisition using a lorentz-force actuated jet injector. *Journal of Controlled Release* **2015**, *211*, 37-43.
54. Pu, Z.; Zou, C.; Wang, R.; Lai, X.; Yu, H.; Xu, K.; Li, D. A continuous glucose monitoring device by graphene modified electrochemical sensor in microfluidic system. *Biomicrofluidics* **2016**, *10*, 011910.
55. Soto, F.; Mishra, R.K.; Chrostowski, R.; Martin, A.; Wang, J. Epidermal Tattoo Patch for Ultrasound-Based Transdermal Microballistic Delivery. *Advanced Materials Technologies* **2017**, *2*, 1700210.

56. Mitragotri, S.; Coleman, M.; Kost, J.; Langer, R. Analysis of ultrasonically extracted interstitial fluid as a predictor of blood glucose levels. *Journal of Applied Physiology* **2000**.
57. Liu, Y.; Huang, B.; Yao, Y. Micromachined biosensor system for interstitial fluid sampling and glucose monitoring. In Proceedings of the 2012 IEEE International Conference on Mechatronics and Automation, 2012; pp. 647-652.
58. Ulrich, J.D.; Burchett, J.M.; Restivo, J.L.; Schuler, D.R.; Verghese, P.B.; Mahan, T.E.; Landreth, G.E.; Castellano, J.M.; Jiang, H.; Cirrito, J.R. In vivo measurement of apolipoprotein E from the brain interstitial fluid using microdialysis. *Molecular neurodegeneration* **2013**, *8*, 1-7.
59. Wiig, H.; Swartz, M.A. Interstitial fluid and lymph formation and transport: physiological regulation and roles in inflammation and cancer. *Physiological reviews* **2012**, *92*, 1005-1060.
60. Miller, P.R.; Taylor, R.M.; Tran, B.Q.; Boyd, G.; Glaros, T.; Chavez, V.H.; Krishnakumar, R.; Sinha, A.; Poorey, K.; Williams, K.P. Extraction and biomolecular analysis of dermal interstitial fluid collected with hollow microneedles. *Communications Biology* **2018**, *1*, 1-11.
61. Takeuchi, K.; Takama, N.; Kim, B.; Sharma, K.; Ruther, P.; Paul, O. A Porous Microneedle Array Connected to Microfluidic System for ISF Collection. In Proceedings of the 2018 IEEE CPMT Symposium Japan (ICSJ), 2018; pp. 85-88.
62. Wang, P.M.; Cornwell, M.; Prausnitz, M.R. Minimally invasive extraction of dermal interstitial fluid for glucose monitoring using microneedles. *Diabetes technology & therapeutics* **2005**, *7*, 131-141.
63. Mukerjee, E.; Collins, S.; Isseroff, R.R.; Smith, R. Microneedle array for transdermal biological fluid extraction and in situ analysis. *Sensors and Actuators A: Physical* **2004**, *114*, 267-275.
64. Ventrelli, L.; Marsilio Strambini, L.; Barillaro, G. Microneedles for transdermal biosensing: current picture and future direction. *Adv Healthc Mater* **2015**, *4*, 2606-2640.
65. He, R.; Niu, Y.; Li, Z.; Li, A.; Yang, H.; Xu, F.; Li, F. A Hydrogel Microneedle Patch for Point-of-Care Testing Based on Skin Interstitial Fluid. *Adv Healthc Mater* **2020**, *9*, 1901201.
66. Zheng, M.; Wang, Z.; Chang, H.; Wang, L.; Chew, S.W.; Lio, D.C.S.; Cui, M.; Liu, L.; Tee, B.C.; Xu, C. Osmosis-Powered Hydrogel Microneedles for Microliters of Skin Interstitial Fluid Extraction within Minutes. *Adv Healthc Mater* **2020**, *9*, 1901683.
67. Nguyen, N.-T.; Wereley, S.T.; Shaegh, S.A.M. *Fundamentals and applications of microfluidics*; Artech house: 2019.
68. Davis, S.P.; Landis, B.J.; Adams, Z.H.; Allen, M.G.; Prausnitz, M.R. Insertion of microneedles into skin: measurement and prediction of insertion force and needle fracture force. *Journal of Biomechanics* **2004**, *37*, 1155-1163, doi:https://doi.org/10.1016/j.jbiomech.2003.12.010.
69. Use of International Standard ISO 10993-1, "Biological evaluation of medical devices - Part 1: Evaluation and testing within a risk management process". *U.S. Food and Drug Administration (FDA)* **September 4, 2020**.
70. Wu, Y.; Qiu, Y.; Zhang, S.; Qin, G.; Gao, Y. Microneedle-based drug delivery: studies on delivery parameters and biocompatibility. *Biomed Microdevices* **2008**, *10*, 601-610, doi:10.1007/s10544-008-9171-x.
71. Schossleitner, K.; O'Mahony, C.; Brandstatter, S.; Haslinger, M.J.; Demuth, S.; Fechtig, D.; Petzelbauer, P. Differences in biocompatibility of microneedles from cyclic olefin polymers with human endothelial and epithelial skin cells. *J Biomed Mater Res A* **2019**, *107*, 505-512, doi:10.1002/jbm.a.36565.
72. Moussi, K.; Bukhamsin, A.; Hidalgo, T.; Kosel, J. Biocompatible 3D Printed Microneedles for Transdermal, Intradermal, and Percutaneous Applications. *Advanced Engineering Materials* **2019**, *22*, 1901358, doi:10.1002/adem.201901358.
73. CT Hanks , J.W., Z Sun . In vitro models of biocompatibility: a review. *Dent Mater* **1996**, *12*, 186-193.
74. Wataha, J.C. Principles of biocompatibility for dental practitioners. *The Journal of Prosthetic Dentistry* **2001**, 203-209.
75. Yadav, S.; Vadivelu, R.; Ahmed, M.; Barton, M.; Nguyen, N.-T. Stretching cells - An approach for early cancer diagnosis. *Exp Cell Res* **2019**, *378*, 191-197, doi:10.1016/j.yexcr.2019.01.029.
76. Yadav, S.; Barton, M.; Nguyen, N.-T. Stretching Induces Overexpression of RhoA and Rac1 GTPases in Breast Cancer Cells. *Adv. Biosyst.* **2019**, doi:10.1002/adbi.201900222.

77. Soenen, S.J.; Manshian, B.; Montenegro, J.M.; Amin, F.; Meermann, B.r.; Thiron, T.; Cornelissen, M.; Vanhaecke, F.; Doak, S.; Wolfgang J. Parak; et al. Cytotoxic Effects of Gold Nanoparticles: A Multiparametric Study. *ACS Nano* **2012**, *6*, 5767-5783.
78. Riss, T.; Niles, A.; Moravec, R.; Karassina, N.; Vidugiriene, J. Cytotoxicity Assays: In Vitro Methods to Measure Dead Cells. *The Assay Guidance Manual* **2019**.
79. Weber, M.; Steinle, H.; Golombek, S.; Hann, L.; Schlensak, C.; Wendel, H.P.; Avci-Adali, M. Blood-Contacting Biomaterials: In Vitro Evaluation of the Hemocompatibility. *Front. Bioeng. Biotechnol.* **2018**, *6*.
80. McGarry, H.F. The murine local lymph node assay: Regulatory and potency considerations under REACH. *Toxicology* **2007**, *238*, 71-89.
81. Larraneta, E.; Lutton, R.E.; Woolfson, A.D.; Donnelly, R.F. Microneedle arrays as transdermal and intradermal drug delivery systems: Materials science, manufacture and commercial development. *Materials Science and Engineering: R: Reports* **2016**, *104*, 1-32.
82. Hegarty, C.; McKillop, S.; Dooher, T.; Dixon, D.; Davis, J. Composite Microneedle Arrays Modified With Palladium Nanoclusters for Electrocatalytic Detection of Peroxide. *IEEE Sensors Letters* **2019**, *3*, 1-4.
83. Gowers, S.A.; Freeman, D.M.; Rawson, T.M.; Rogers, M.L.; Wilson, R.C.; Holmes, A.H.; Cass, A.E.; O'Hare, D. Development of a minimally invasive microneedle-based sensor for continuous monitoring of β-lactam antibiotic concentrations in vivo. *ACS sensors* **2019**, *4*, 1072-1080.
84. Jenkins, D.; Corrie, S.; Flaim, C.; Kendall, M. High density and high aspect ratio solid micro-nanoprojection arrays for targeted skin vaccine delivery and specific antibody extraction. *Rsc Advances* **2012**, *2*, 3490-3495.
85. Lee, S.J.; Yoon, H.S.; Xuan, X.; Park, J.Y.; Paik, S.-J.; Allen, M.G. A patch type non-enzymatic biosensor based on 3D SUS micro-needle electrode array for minimally invasive continuous glucose monitoring. *Sensors and Actuators B: Chemical* **2016**, *222*, 1144-1151.
86. Berry, C.A.; Smith, Z.R.; Collins, S.D.; Smith, R.L. Dermal ISF Collection Using a Si Microneedle Array. In Proceedings of the 2020 IEEE 33rd International Conference on Micro Electro Mechanical Systems (MEMS), 2020; pp. 365-368.
87. Chua, B.; Desai, S.P.; Tierney, M.J.; Tamada, J.A.; Jina, A.N. Effect of microneedles shape on skin penetration and minimally invasive continuous glucose monitoring in vivo. *Sensors and Actuators A: Physical* **2013**, *203*, 373-381.
88. Mansoor, I.; Liu, Y.; Häfeli, U.; Stoeber, B. Arrays of hollow out-of-plane microneedles made by metal electrodeposition onto solvent cast conductive polymer structures. *Journal of Micromechanics and Microengineering* **2013**, *23*, 085011.
89. Chen, J.; Wang, M.; Ye, Y.; Yang, Z.; Ruan, Z.; Jin, N. Fabrication of sponge-forming microneedle patch for rapidly sampling interstitial fluid for analysis. *Biomedical microdevices* **2019**, *21*, 63.
90. Chang, H.; Zheng, M.; Yu, X.; Than, A.; Seeni, R.Z.; Kang, R.; Tian, J.; Khanh, D.P.; Liu, L.; Chen, P. A swellable microneedle patch to rapidly extract skin interstitial fluid for timely metabolic analysis. *Advanced Materials* **2017**, *29*, 1702243.
91. Sakaguchi, K.; Hirota, Y.; Hashimoto, N.; Ogawa, W.; Sato, T.; Okada, S.; Hagino, K.; Asakura, Y.; Kikkawa, Y.; Kojima, J. A minimally invasive system for glucose area under the curve measurement using interstitial fluid extraction technology: evaluation of the accuracy and usefulness with oral glucose tolerance tests in subjects with and without diabetes. *Diabetes Technology & Therapeutics* **2012**, *14*, 485-491.
92. Ito, Y.; Inagaki, Y.; Kobuchi, S.; Takada, K.; Sakaeda, T. Therapeutic drug monitoring of vancomycin in dermal interstitial fluid using dissolving microneedles. *International journal of medical sciences* **2016**, *13*, 271.
93. Anderson, A.; Hegarty, C.; Casimero, C.; Davis, J. Electrochemically Controlled Dissolution of Nanocarbon–Cellulose Acetate Phthalate Microneedle Arrays. *ACS applied materials & interfaces* **2019**, *11*, 35540-35547.
94. Barrett, C.; O'Sullivan, F.; Barry, S.; Grygoryev, K.; O'Gorman, D.; O'Mahony, C.; O'Riordan, A. Novel Surface Modified Polymer Microneedle based Biosensors for Interstitial Fluid Glucose Detection. In Proceedings of the 2019 IEEE SENSORS, 2019; pp. 1-4.
95. Park, J.E.; Yonet-Tanyeri, N.; Vander Ende, E.; Henry, A.-I.; Perez White, B.E.; Mrksich, M.; Van Duyne, R.P. Plasmonic microneedle arrays for in situ sensing with surface-enhanced Raman spectroscopy (SERS). *Nano letters* **2019**, *19*, 6862-6868.

96. Ju, J.; Hsieh, C.-m.; Tian, Y.; Kang, J.; Chia, R.; Chang, H.; Bai, Y.; Xu, C.; Wang, X.; Liu, Q. Surface Enhanced Raman Spectroscopy based Biosensor with a Microneedle Array for Minimally Invasive In Vivo Glucose Measurements. *ACS Sensors* **2020**.

97. Mandal, A.; Boopathy, A.V.; Lam, L.K.; Moynihan, K.D.; Welch, M.E.; Bennett, N.R.; Turvey, M.E.; Thai, N.; Van, J.H.; Love, J.C. Cell and fluid sampling microneedle patches for monitoring skin-resident immunity. *Science translational medicine* **2018**, *10*.

98. Al Sulaiman, D.; Chang, J.Y.; Bennett, N.R.; Topouzi, H.; Higgins, C.A.; Irvine, D.J.; Ladame, S. Hydrogel-coated microneedle arrays for minimally invasive sampling and sensing of specific circulating nucleic acids from skin interstitial fluid. *ACS nano* **2019**, *13*, 9620-9628.

99. Samavat, S.; Lloyd, J.; O'Dea, L.; Zhang, W.; Preedy, E.; Luzio, S.; Teng, K.S. Uniform sensing layer of immiscible enzyme-mediator compounds developed via a spray aerosol mixing technique towards low cost minimally invasive microneedle continuous glucose monitoring devices. *Biosensors and Bioelectronics* **2018**, *118*, 224-230.

100. Zhang, X.; Chen, G.; Bian, F.; Cai, L.; Zhao, Y. Encoded microneedle arrays for detection of skin interstitial fluid biomarkers. *Advanced Materials* **2019**, *31*, 1902825.

101. Senel, M.; Dervisevic, M.; Voelcker, N.H. Gold microneedles fabricated by casting of gold ink used for urea sensing. *Materials Letters* **2019**, *243*, 50-53.

102. Cass, A.E.; Sharma, S. Microneedle enzyme sensor arrays for continuous in vivo monitoring. In *Methods in enzymology*; Elsevier: 2017; Volume 589, pp. 413-427.

103. Rawson, T.M.; Sharma, S.; Georgiou, P.; Holmes, A.; Cass, A.; O'Hare, D. Towards a minimally invasive device for beta-lactam monitoring in humans. *Electrochemistry communications* **2017**, *82*, 1-5.

104. Sharma, S.; Saeed, A.; Johnson, C.; Gadegaard, N.; Cass, A.E. Rapid, low cost prototyping of transdermal devices for personal healthcare monitoring. *Sensing and Bio-Sensing Research* **2017**, *13*, 104-108.

105. Bollella, P.; Sharma, S.; Cass, A.E.G.; Antiochia, R. Microneedle-based biosensor for minimally-invasive lactate detection. *Biosensors and Bioelectronics* **2019**, *123*, 152-159.

106. Rawson, T.M.; Gowers, S.A.; Freeman, D.M.; Wilson, R.C.; Sharma, S.; Gilchrist, M.; MacGowan, A.; Lovering, A.; Bayliss, M.; Kyriakides, M. Microneedle biosensors for real-time, minimally invasive drug monitoring of phenoxymethylpenicillin: a first-in-human evaluation in healthy volunteers. *The Lancet Digital Health* **2019**, *1*, e335-e343.

107. Bollella, P.; Sharma, S.; Cass, A.E.; Tasca, F.; Antiochia, R. Minimally invasive glucose monitoring using a highly porous gold microneedles-based biosensor: Characterization and application in artificial interstitial fluid. *Catalysts* **2019**, *9*, 580.

108. Coffey, J.W.; Corrie, S.R.; Kendall, M.A. Early circulating biomarker detection using a wearable microprojection array skin patch. *Biomaterials* **2013**, *34*, 9572-9583.

109. Coffey, J.W.; Meliga, S.C.; Corrie, S.R.; Kendall, M.A. Dynamic application of microprojection arrays to skin induces circulating protein extravasation for enhanced biomarker capture and detection. *Biomaterials* **2016**, *84*, 130-143.

110. Coffey, J.W.; Corrie, S.R.; Kendall, M.A. Rapid and selective sampling of IgG from skin in less than 1 min using a high surface area wearable immunoassay patch. *Biomaterials* **2018**, *170*, 49-57.

111. Chinnadayyala, S.R.; Park, I.; Cho, S. Nonenzymatic determination of glucose at near neutral pH values based on the use of nafion and platinum black coated microneedle electrode array. *Microchimica Acta* **2018**, *185*, 250.

112. Kolluru, C.; Williams, M.; Chae, J.; Prausnitz, M.R. Recruitment and collection of dermal interstitial fluid using a microneedle patch. *Advanced healthcare materials* **2019**, *8*, 1801262.

113. Kolluru, C.; Williams, M.; Yeh, J.S.; Noel, R.K.; Knaack, J.; Prausnitz, M.R. Monitoring drug pharmacokinetics and immunologic biomarkers in dermal interstitial fluid using a microneedle patch. *Biomedical microdevices* **2019**, *21*, 14.

114. Griss, P.; Stemme, G. Side-opened out-of-plane microneedles for microfluidic transdermal liquid transfer. *Journal of Microelectromechanical systems* **2003**, *12*, 296-301.

115. Roxhed, N.; Gasser, T.C.; Griss, P.; Holzapfel, G.A.; Stemme, G. Penetration-enhanced ultrasharp microneedles and prediction on skin interaction for efficient transdermal drug delivery. *Journal of Microelectromechanical systems* **2007**, *16*, 1429-1440.

116. Windmiller, J.R.; Zhou, N.; Chuang, M.-C.; Valdés-Ramírez, G.; Santhosh, P.; Miller, P.R.; Narayan, R.; Wang, J. Microneedle array-based carbon paste amperometric sensors and biosensors. *Analyst* **2011**, *136*, 1846-1851.

117. Miller, P.R.; Gittard, S.D.; Edwards, T.L.; Lopez, D.M.; Xiao, X.; Wheeler, D.R.; Monteiro-Riviere, N.A.; Brozik, S.M.; Polsky, R.; Narayan, R.J. Integrated carbon fiber electrodes within hollow polymer microneedles for transdermal electrochemical sensing. *Biomicrofluidics* **2011**, *5*, 013415.

118. Jina, A.; Tierney, M.J.; Tamada, J.A.; McGill, S.; Desai, S.; Chua, B.; Chang, A.; Christiansen, M. Design, development, and evaluation of a novel microneedle array-based continuous glucose monitor. *Journal of diabetes science and technology* **2014**, *8*, 483-487.

119. Ranamukhaarachchi, S.A.; Padeste, C.; Dübner, M.; Häfeli, U.O.; Stoeber, B.; Cadarso, V.J. Integrated hollow microneedle-optofluidic biosensor for therapeutic drug monitoring in sub-nanoliter volumes. *Scientific reports* **2016**, *6*, 29075.

120. Ranamukhaarachchi, S.A.; Padeste, C.; Häfeli, U.O.; Stoeber, B.; Cadarso, V.J. Design considerations of a hollow microneedle-optofluidic biosensing platform incorporating enzyme-linked assays. *Journal of Micromechanics and Microengineering* **2017**, *28*, 024002.

121. Ribet, F.; Stemme, G.; Roxhed, N. Microneedle-based system for minimally invasive continuous monitoring of glucose in the dermal interstitial fluid. In Proceedings of the 2018 IEEE Micro Electro Mechanical Systems (MEMS), 2018; pp. 408-411.

122. Nicholas, D.; Logan, K.A.; Sheng, Y.; Gao, J.; Farrell, S.; Dixon, D.; Callan, B.; McHale, A.P.; Callan, J.F. Rapid paper based colorimetric detection of glucose using a hollow microneedle device. *International journal of pharmaceutics* **2018**, *547*, 244-249.

123. Zhao, L.; Wen, Z.; Jiang, F.; Zheng, Z.; Lu, S. Silk/polyols/GOD microneedle based electrochemical biosensor for continuous glucose monitoring. *RSC Advances* **2020**, *10*, 6163-6171.

124. Miller, P.R.; Xiao, X.; Brener, I.; Burckel, D.B.; Narayan, R.; Polsky, R. Microneedle-Based Transdermal Sensor for On-Chip Potentiometric Determination of K+. *Adv Healthc Mater* **2014**, *3*, 876-881.

125. Mohan, A.V.; Windmiller, J.R.; Mishra, R.K.; Wang, J. Continuous minimally-invasive alcohol monitoring using microneedle sensor arrays. *Biosensors and Bioelectronics* **2017**, *91*, 574-579.

126. Ciui, B.; Martin, A.; Mishra, R.K.; Brunetti, B.; Nakagawa, T.; Dawkins, T.J.; Lyu, M.; Cristea, C.; Sandulescu, R.; Wang, J. Wearable wireless tyrosinase bandage and microneedle sensors: toward melanoma screening. *Adv Healthc Mater* **2018**, *7*, 1701264.

127. Teymourian, H.; Moonla, C.; Tehrani, F.; Vargas, E.; Aghavali, R.; Barfidokht, A.; Tangkuaram, T.; Mercier, P.P.; Dassau, E.; Wang, J. Microneedle-Based Detection of Ketone Bodies along with Glucose and Lactate: Toward Real-Time Continuous Interstitial Fluid Monitoring of Diabetic Ketosis and Ketoacidosis. *Analytical Chemistry* **2019**, *92*, 2291-2300.

128. Tran, B.Q.; Miller, P.R.; Taylor, R.M.; Boyd, G.; Mach, P.M.; Rosenzweig, C.N.; Baca, J.T.; Polsky, R.; Glaros, T. Proteomic characterization of dermal interstitial fluid extracted using a novel microneedle-assisted technique. *Journal of proteome research* **2018**, *17*, 479-485.

129. Liu, L.; Kai, H.; Nagamine, K.; Ogawa, Y.; Nishizawa, M. Porous polymer microneedles with interconnecting microchannels for rapid fluid transport. *RSC advances* **2016**, *6*, 48630-48635.

130. Lee, H.; Takeuchi, K.; Sasaki, Y.; Takama, N.; Minami, T.; Kim, B. Porous Microneedle Integrated in Paper based Glucose Sensor for Fluid Channel Interface. In Proceedings of the 2019 IEEE CPMT Symposium Japan (ICSJ), 2019; pp. 39-42.

131. Gholami, S.; Mohebi, M.-M.; Hajizadeh-Saffar, E.; Ghanian, M.-H.; Zarkesh, I.; Baharvand, H. Fabrication of microporous inorganic microneedles by centrifugal casting method for transdermal extraction and delivery. *International journal of pharmaceutics* **2019**, *558*, 299-310.

132. Nagamine, K.; Kubota, J.; Kai, H.; Ono, Y.; Nishizawa, M. An array of porous microneedles for transdermal monitoring of intercellular swelling. *Biomedical microdevices* **2017**, *19*, 68.

133. Morishita, Y.; Takama, N.; Kim, B. Fabrication of porous biodegradable microneedles for glucose monitoring sensor. In Proceedings of the 2018 IEEE CPMT Symposium Japan (ICSJ), 2018; pp. 81-84.

134. Zhu, J.; Zhou, X.; Kim, H.J.; Qu, M.; Jiang, X.; Lee, K.; Ren, L.; Wu, Q.; Wang, C.; Zhu, X. Gelatin Methacryloyl Microneedle Patches for Minimally Invasive Extraction of Skin Interstitial Fluid. *Small* **2020**, *16*, 1905910.

135. Donnelly, R.F.; Mooney, K.; Mccrudden, M.T.; Vicente-Pérez, E.M.; Belaid, L.; González-Vázquez, P.; Mcelnay, J.C.; Woolfson, A.D. Hydrogel-forming microneedles increase in volume during swelling in skin, but skin barrier function recovery is unaffected. *Journal of pharmaceutical sciences* **2014**, *103*, 1478-1486.

136. Romanyuk, A.V.; Zvezdin, V.N.; Samant, P.; Grenader, M.I.; Zemlyanova, M.; Prausnitz, M.R. Collection of analytes from microneedle patches. *Analytical Chemistry* **2014**, *86*, 10520-10523.

137. Caffarel-Salvador, E.; Brady, A.J.; Eltayib, E.; Meng, T.; Alonso-Vicente, A.; Gonzalez-Vazquez, P.; Torrisi, B.M.; Vicente-Perez, E.M.; Mooney, K.; Jones, D.S. Hydrogel-forming microneedle arrays allow detection of drugs and glucose in vivo: potential for use in diagnosis and therapeutic drug monitoring. *PloS one* **2015**, *10*, e0145644.

138. Eltayib, E.; Brady, A.J.; Caffarel-Salvador, E.; Gonzalez-Vazquez, P.; Alkilani, A.Z.; McCarthy, H.O.; McElnay, J.C.; Donnelly, R.F. Hydrogel-forming microneedle arrays: potential for use in minimally-invasive lithium monitoring. *European Journal of Pharmaceutics and Biopharmaceutics* **2016**, *102*, 123-131.

139. Tejavibulya, N.; Colburn, D.A.; Marcogliese, F.A.; Yang, K.-A.; Guo, V.; Chowdhury, S.; Stojanovic, M.N.; Sia, S.K. Hydrogel Microfilaments toward Intradermal Health Monitoring. *Iscience* **2019**, *21*, 328-340.

140. Fonseca, D.F.; Costa, P.C.; Almeida, I.F.; Dias-Pereira, P.; Correia-Sá, I.; Bastos, V.; Oliveira, H.; Vilela, C.; Silvestre, A.J.; Freire, C.S. Swellable Gelatin Methacryloyl Microneedles for Extraction of Interstitial Skin Fluid toward Minimally Invasive Monitoring of Urea. *Macromolecular Bioscience* **2020**, 2000195.

141. Yang, B.; Fang, X.; Kong, J. In Situ Sampling and Monitoring Cell-Free DNA of the Epstein–Barr Virus from Dermal Interstitial Fluid Using Wearable Microneedle Patches. *ACS applied materials & interfaces* **2019**, *11*, 38448-38458.

142. Zhang, J.; Hao, N.; Liu, W.; Lu, M.; Sun, L.; Chen, N.; Wu, M.; Zhao, X.; Xing, B.; Sun, W.; et al. In-depth proteomic analysis of tissue interstitial fluid for hepatocellular carcinoma serum biomarker discovery. *Br J Cancer* **2017**, *117*, 1676-1684, doi:10.1038/bjc.2017.344.

143. Ahn, S.-M.; Simpson, R.J. Body fluid proteomics: Prospects for biomarker discovery. *PROTEOMICS – Clinical Applications* **2007**, *1*, 1004-1015, doi:https://doi.org/10.1002/prca.200700217.

144. Miller, P.R.; Taylor, R.M.; Tran, B.Q.; Boyd, G.; Glaros, T.; Chavez, V.H.; Krishnakumar, R.; Sinha, A.; Poorey, K.; Williams, K.P.; et al. Extraction and biomolecular analysis of dermal interstitial fluid collected with hollow microneedles. *Communications Biology* **2018**, *1*, 173, doi:10.1038/s42003-018-0170-z.

145. Celis, J.E.; Gromov, P.; Cabezón, T.; Moreira, J.M.A.; Ambartsumian, N.; Sandelin, K.; Rank, F.; Gromova, I. Proteomic Characterization of the Interstitial Fluid Perfusing the Breast Tumor Microenvironment: A Novel Resource for Biomarker and Therapeutic Target Discovery**This work was supported by the Danish Cancer Society through the budget of the Institute of Cancer Biology and by grants from the Danish Medical Research Council, the Natural Science and Medical Committee of the Danish Cancer Society, Novo Nordisk, and the John and Birthe Meyer Foundation. The support from the Marketing Department at the Danish Cancer Society is also greatly appreciated. We would also like to acknowledge the support and collaboration of Eurogentec. The costs of publication of this article were defrayed in part by the payment of page charges. This article must therefore be hereby marked "advertisement" in accordance with 18 U.S.C. Section 1734 solely to indicate this fact. *Molecular & Cellular Proteomics* **2004**, *3*, 327-344, doi:https://doi.org/10.1074/mcp.M400009-MCP200.

146. Halvorsen, A.R.; Helland, Å.; Gromov, P.; Wielenga, V.T.; Talman, M.-L.M.; Brunner, N.; Sandhu, V.; Børresen-Dale, A.-L.; Gromova, I.; Haakensen, V.D. Profiling of microRNAs in tumor interstitial fluid of breast tumors – a novel resource to identify biomarkers for prognostic classification and detection of cancer. *Molecular Oncology* **2017**, *11*, 220-234, doi:https://doi.org/10.1002/1878-0261.12025.

147. Nilsson, A.K.; Sjöbom, U.; Christenson, K.; Hellström, A. Lipid profiling of suction blister fluid: comparison of lipids in interstitial fluid and plasma. *Lipids in Health and Disease* **2019**, *18*, 164, doi:10.1186/s12944-019-1107-3.

148. Espinoza, J.A.; Jabeen, S.; Batra, R.; Papaleo, E.; Haakensen, V.; Timmermans Wielenga, V.; Møller Talman, M.-L.; Brunner, N.; Børresen-Dale, A.-L.; Gromov, P.; et al. Cytokine profiling of tumor interstitial fluid of the breast and its relationship with lymphocyte infiltration and clinicopathological characteristics. *OncoImmunology* **2016**, *5*, e1248015, doi:10.1080/2162402X.2016.1248015.

149. Sun, W.; Ma, J.; Wu, S.; Yang, D.; Yan, Y.; Liu, K.; Wang, J.; Sun, L.; Chen, N.; Wei, H.; et al. Characterization of the Liver Tissue Interstitial Fluid (TIF) Proteome Indicates Potential for Application in Liver Disease Biomarker Discovery. *Journal of Proteome Research* **2010**, *9*, 1020-1031, doi:10.1021/pr9009172.

150. Madden, J.; O'Mahony, C.; Thompson, M.; O'Riordan, A.; Galvin, P. Biosensing in dermal interstitial fluid using microneedle based electrochemical devices. *Sensing and Bio-Sensing Research* **2020**, *29*, 100348, doi:https://doi.org/10.1016/j.sbsr.2020.100348.

151. Zimmermann, S.; Fienbork, D.; Stoeber, B.; Flounders, A.W.; Liepmann, D. A microneedle-based glucose monitor: fabricated on a wafer-level using in-device enzyme immobilization. In Proceedings of the TRANSDUCERS '03. 12th International Conference on Solid-State Sensors, Actuators and Microsystems. Digest of Technical Papers (Cat. No.03TH8664), 8-12 June 2003, 2003; pp. 99-102 vol.101.

152. Wang, J. Electrochemical Glucose Biosensors. *Chemical Reviews* **2008**, *108*, 814-825, doi:10.1021/cr068123a.

153. Miller, P.R.; Skoog, S.A.; Edwards, T.L.; Lopez, D.M.; Wheeler, D.R.; Arango, D.C.; Xiao, X.; Brozik, S.M.; Wang, J.; Polsky, R.; et al. Multiplexed microneedle-based biosensor array for characterization of metabolic acidosis. *Talanta* **2012**, *88*, 739-742, doi:https://doi.org/10.1016/j.talanta.2011.11.046.

154. Valdés-Ramírez, G.; Li, Y.-C.; Kim, J.; Jia, W.; Bandodkar, A.J.; Nuñez-Flores, R.; Miller, P.R.; Wu, S.-Y.; Narayan, R.; Windmiller, J.R.; et al. Microneedle-based self-powered glucose sensor. *Electrochemistry Communications* **2014**, *47*, 58-62, doi:https://doi.org/10.1016/j.elecom.2014.07.014.

155. Goud, K.Y.; Moonla, C.; Mishra, R.K.; Yu, C.; Narayan, R.; Litvan, I.; Wang, J. Wearable Electrochemical Microneedle Sensor for Continuous Monitoring of Levodopa: Toward Parkinson Management. *ACS Sensors* **2019**, *4*, 2196-2204, doi:10.1021/acssensors.9b01127.

156. Teymourian, H.; Moonla, C.; Tehrani, F.; Vargas, E.; Aghavali, R.; Barfidokht, A.; Tangkuaram, T.; Mercier, P.P.; Dassau, E.; Wang, J. Microneedle-Based Detection of Ketone Bodies along with Glucose and Lactate: Toward Real-Time Continuous Interstitial Fluid Monitoring of Diabetic Ketosis and Ketoacidosis. *Analytical Chemistry* **2020**, *92*, 2291-2300, doi:10.1021/acs.analchem.9b05109.

157. Barrett, C.; Dawson, K.; O'Mahony, C.; O'Riordan, A. Development of Low Cost Rapid Fabrication of Sharp Polymer Microneedles for In Vivo Glucose Biosensing Applications. *ECS Journal of Solid State Science and Technology* **2015**, *4*, S3053-S3058, doi:10.1149/2.0141510jss.

158. Chen, D.; Wang, C.; Chen, W.; Chen, Y.; Zhang, J.X.J. PVDF-Nafion nanomembranes coated microneedles for in vivo transcutaneous implantable glucose sensing. *Biosensors and Bioelectronics* **2015**, *74*, 1047-1052, doi:https://doi.org/10.1016/j.bios.2015.07.036.

159. Caliò, A.; Dardano, P.; Di Palma, V.; Bevilacqua, M.F.; Di Matteo, A.; Iuele, H.; De Stefano, L. Polymeric microneedles based enzymatic electrodes for electrochemical biosensing of glucose and lactic acid. *Sensors and Actuators B: Chemical* **2016**, *236*, 343-349, doi:https://doi.org/10.1016/j.snb.2016.05.156.

160. Sharma, S.; Huang, Z.; Rogers, M.; Boutelle, M.; Cass, A.E.G. Evaluation of a minimally invasive glucose biosensor for continuous tissue monitoring. *Analytical and Bioanalytical Chemistry* **2016**, *408*, 8427-8435, doi:10.1007/s00216-016-9961-6.

161. Skoog, S.A.; Miller, P.R.; Boehm, R.D.; Sumant, A.V.; Polsky, R.; Narayan, R.J. Nitrogen-incorporated ultrananocrystalline diamond microneedle arrays for electrochemical biosensing. *Diamond and Related Materials* **2015**, *54*, 39-46, doi:https://doi.org/10.1016/j.diamond.2014.11.016.

162. McConville, A.; Davis, J. Transdermal microneedle sensor arrays based on palladium: Polymer composites. *Electrochemistry Communications* **2016**, *72*, 162-165, doi:https://doi.org/10.1016/j.elecom.2016.09.024.

163. Hegarty, C.; McConville, A.; McGlynn, R.J.; Mariotti, D.; Davis, J. Design of composite microneedle sensor systems for the measurement of transdermal pH. *Materials Chemistry and Physics* **2019**, *227*, 340-346, doi:https://doi.org/10.1016/j.matchemphys.2019.01.052.

164. Vazquez, P.; Herzog, G.; O'Mahony, C.; O'Brien, J.; Scully, J.; Blake, A.; O'Mathuna, C.; Galvin, P. Microscopic gel–liquid interfaces supported by hollow microneedle array for voltammetric drug detection. *Sensors and Actuators B: Chemical* **2014**, *201*, 572-578, doi:https://doi.org/10.1016/j.snb.2014.04.080.

165. Kolluru, C.; Gupta, R.; Jiang, Q.; Williams, M.; Gholami Derami, H.; Cao, S.; Noel, R.K.; Singamaneni, S.; Prausnitz, M.R. Plasmonic Paper Microneedle Patch for On-Patch Detection of Molecules in Dermal Interstitial Fluid. *ACS sensors* **2019**, *4*, 1569-1576.

166. Trzebinski, J.; Sharma, S.; Moniz, A.R.-B.; Michelakis, K.; Zhang, Y.; Cass, A.E. Microfluidic device to investigate factors affecting performance in biosensors designed for transdermal applications. *Lab on a Chip* **2012**, *12*, 348-352.

167. Martín, A.; Kim, J.; Kurniawan, J.F.; Sempionatto, J.R.; Moreto, J.R.; Tang, G.; Campbell, A.S.; Shin, A.; Lee, M.Y.; Liu, X. Epidermal microfluidic electrochemical detection system: Enhanced sweat sampling and metabolite detection. *ACS sensors* **2017**, *2*, 1860-1868.

168. Munaz, A.; Shiddiky, M.J.; Nguyen, N.-T. Recent advances and current challenges in magnetophoresis based micro magnetofluidics. *Biomicrofluidics* **2018**, *12*, 031501.

169. Larrañeta, E.; Moore, J.; Vicente-Pérez, E.M.; González-Vázquez, P.; Lutton, R.; Woolfson, A.D.; Donnelly, R.F. A proposed model membrane and test method for microneedle insertion studies. *International journal of pharmaceutics* **2014**, *472*, 65-73.

170. Ribet, F.; Dobielewski, M.; Böttcher, M.; Beck, O.; Stemme, G.; Roxhed, N. Minimally invasive and volume-metered extraction of interstitial fluid: bloodless point-of-care sampling for bioanalyte detection. **2020**.

171. Wang, S.; Tarbell, J.M. Effect of fluid flow on smooth muscle cells in a 3-dimensional collagen gel model. *Arteriosclerosis, thrombosis, and vascular biology* **2000**, *20*, 2220-2225.

172. Wufuer, M.; Lee, G.; Hur, W.; Jeon, B.; Kim, B.J.; Choi, T.H.; Lee, S. Skin-on-a-chip model simulating inflammation, edema and drug-based treatment. *Scientific reports* **2016**, *6*, 37471.

173. Munaz, A.; Vadivelu, R.K.; John, J.S.; Barton, M.; Kamble, H.; Nguyen, N.-T. Three-dimensional printing of biological matters. *Journal of Science: Advanced Materials and Devices* **2016**, *1*, 1-17.

174. Kimura, H.; Sakai, Y.; Fujii, T. Organ/body-on-a-chip based on microfluidic technology for drug discovery. *Drug metabolism and pharmacokinetics* **2018**, *33*, 43-48.

175. Sriram, G.; Alberti, M.; Dancik, Y.; Wu, B.; Wu, R.; Feng, Z.; Ramasamy, S.; Bigliardi, P.L.; Bigliardi-Qi, M.; Wang, Z. Full-thickness human skin-on-chip with enhanced epidermal morphogenesis and barrier function. *Materials Today* **2018**, *21*, 326-340.

176. Munaz, A.; Vadivelu, R.K.; St John, J.A.; Nguyen, N.-T. A lab-on-a-chip device for investigating the fusion process of olfactory ensheathing cell spheroids. *Lab on a Chip* **2016**, *16*, 2946-2954.

177. Zhang, Q.; Sito, L.; Mao, M.; He, J.; Zhang, Y.S.; Zhao, X. Current advances in skin-on-a-chip models for drug testing. **2018**.